

State-dependent marginal emission factors with autoregressive components

Antonio Panico^{*1,2}, Andrew Burlinson², and Luigi Grossi¹

¹Department of Engineering for Industrial Systems and Technologies,
University of Parma, 43124 Parma, Italy

²School of Economics, University of Sheffield, Sheffield, UK

Abstract

Accurate estimation of Marginal Emission Factors (MEFs) is critical for evaluating the decarbonization potential of low-carbon technologies and demand-side management. However, canonical methodologies, predominantly relying on linear regression and differencing techniques, fail to capture the structural non-linearities inherent in the merit order, i.e. the marginal technology setting electricity prices. Utilizing Markov switching autoregressive models with exogenous regressors (MS-ARX) and hourly US data (2019–2025), we identify distinct, mutually exclusive regimes governed by fuel-price dynamics. We find that linear models overestimate abatement potential by masking the dichotomy between a gas-driven and coal-driven marginal system. Furthermore, using robust structural break detection, we link regime instability to a specific structural shift in natural gas pricing in May 2022. Our results indicate that post-2022, the grid has transitioned into a correction phase where the coal-driven regime is less persistent but highly volatile, necessitating state-dependent policy metrics rather than static annual averages.

Keywords: climate policy, electricity, emissions, regime-switching models, structural break

JEL codes: C22, C51, Q41, Q53

1 Introduction

The United States (U.S.) officially withdrew from the Paris Agreement on January 27, 2026. Marking the second time the nation exited the landmark climate pact under a Trump administration, reaffirming its intent to renege on international legal obligations – including the pledge to halve greenhouse gas emissions by 2030 ([U.S. Department of State, 2021](#)). Despite the [U.S. Department of Energy \(2023\)](#) arguing that achieving 100% clean electricity by 2035 could reduce energy-related emissions by 2.4 gigatons, the path toward deep decarbonization faces renewed uncertainty. Furthermore, established methods

*Email: antonio.panico@unipr.it

overlook inherent non-linearities in the displacement of fossil-fuels at the margin. This is problematic as recent executive orders actively target the revitalization of coal-based power. Our study addresses this critical gap in the literature by providing a robust econometric framework to capture these evolving marginal dynamics.

Policy evaluation often relies on fixed average emission factors (AEF), such as those produced by the [U.S. Environmental Protection Agency \(2019\)](#). Yet, it has become clear that this approach leads to significant (downward) bias, as renewable generation displaces the *marginal* generator rather than the average fuel mix. Accurate estimation of Marginal Emission Factors (MEFs) is therefore essential for evaluating the decarbonization potential of renewable energy, electric vehicles, and demand-side management ([Graff Zivin et al., 2014](#)). Indeed, [Holland et al. \(2022a\)](#) highlighted this tension clearly by showing how MEFs were on the rise in the U.S. despite falling average emissions at least in the short-run. While [Gagnon et al. \(2022\)](#) note the importance of structural change in long-run planning, short-run MEFs remain indispensable for context-dependent near-term operational policies and real-world behavioral responses ([Holland et al., 2022b](#)).

The literature has developed several statistical approaches to estimate MEFs. [Holland and Mansur \(2008\)](#) pioneered a linear regression approach using U.S. data, regressing emissions on generation while controlling for temporal and regional fixed effects. This methodology was widely adopted, most notably by [Callaway et al. \(2018\)](#), [Holladay and LaRiviere \(2017\)](#), and [Holland et al. \(2022a\)](#). In contrast, [Hawkes \(2010\)](#) utilized differencing to represent inter-temporal changes, and [Beltrami et al. \(2020\)](#) utilized time series methods to model autocorrelation in the data-generating process. Although informative, these approaches share a common limitation: they assume a stable, linear relationship between generation and emissions. Moreover, linear techniques estimate an *average* marginal effect. We argue that this fails to capture the inherent non-linearities in merit-order dispatch, where the marginal fossil fuel shifts between “clean” (e.g., natural gas) and “dirty” (e.g., coal) technologies depending on system load and prices.

We address this gap in the literature by utilizing Markov switching autoregressive models with exogenous regressors (MS-ARX)¹ and hourly data for the lower 48 United States (US48). Our work complements relevant literature in which Markov-switching models (MSMs) have been applied in order to model power price forecasts ([Koster and Mosler, 2006](#) and [Kapoor et al., 2023](#)) and wholesale price formation ([Zachmann, 2007](#)). More recently, [Holladay and LaRiviere \(2017\)](#) used MSMs to identify structural breaks in the emissions-gas price relationship following the fracking boom.

More closely related to our study is that of [Ben Amor et al. \(2025\)](#) who suggest that regime-switching frameworks outperform dynamic linear regressions for MEF estimation in the German market. Their Markov switching dynamic regression (MSDR) model finds three regimes representing i) low-emission periods with renewable dominance, ii) high-emission periods characterized by fossil fuel dispatch, and iii) volatile transition states. However, despite finding the emissions and generation series to be stationary, the authors use first-order differences. This transformation is statistically unnecessary for stationary data and introduces interpretational ambiguity by modeling rates of change rather than level-based physical realizations. Another notable limitation of their approach is the use of total generation (including renewables) as the explanatory variable. Since renewable generation contributes zero direct emissions, their regime-switching mechanism distinguishes between periods of high renewable penetration (low MEF) and periods of fossil fuel dominance (high MEF), rather than capturing the shifting marginal dynamics

¹Throughout this work, MS-ARX and MSM are used interchangeably to refer to the same model.

between gas and coal technologies.

Our work overcomes such limitations by simultaneously grounding regime identification in fuel market fundamentals; specifically, we validate that observed regimes correspond to distinct marginal fossil-fuel states² and link regime instability to structural breaks in natural gas pricing. Moreover, our study shows that earlier linear models, despite being less rigorous for estimating MEFs, remain useful for analysing other behaviours of marginal units, specifically the *marginal fuel probability* and *generation-load responsiveness*.

We contribute to the literature in three main ways. First, by rigorous estimation of MEFs for the total US48 region using an MS-ARX framework, allowing us to disentangle distinct, mutually exclusive operating regimes. Second, we demonstrate that standard linear models mask the dichotomy between “clean” (gas-margin) and “dirty” (coal-margin) fossil-fuel states, leading to potential overestimation of abatement potential. Third, we employ a robust structural break detection on natural gas prices to further unpack our regime-switching results. We find that a structural shift in gas pricing in May 2022 fundamentally altered the grid’s stability. Specifically, we observe that after an inflationary phase characterized by energy volatility and rising prices driven by the COVID-19 pandemic and the Ukraine-Russia war, the energy market then entered a correction phase.

The rest of the paper is organized as follows. Section 2 reviews existing MEF estimation methods. Section 3 presents the data, while the empirical methodology is described in Section 4. The results are discussed in Section 5 and Section 6 offers conclusions.

2 Review of existing methods

The extant literature on MEF estimation follows three primary methodological frameworks. First, *US fixed-effects* (US-FE), originating from regression analysis of U.S. inter- and intra-day emissions and generation data while controlling for time and regional fixed effects (Holland and Mansur, 2008, and Callaway et al., 2018). Second, the Hawkes (2010) approach, which employs first-order differencing, capturing system-level changes between settlement periods i.e. intra-day. Third, *ARIMA-FE*, introduced by Beltrami et al. (2020), incorporates autoregressive integrated moving average (ARIMA) components alongside fixed effects within and across days. We will focus on intra-day in what follows, as this underpins our main results, noting that the arguments apply to inter-day, too.

The general *US-FE* specification can be defined as:

$$E_{rt} = \beta_r G_{rt} + \alpha_r + \varepsilon_{rt} \quad (1)$$

where E_{rt} represents emissions in region r at time t , G_{rt} denotes electricity generation, α_r captures regional fixed effects, and β_r is the regional MEF. Since Holland and Mansur (2008) evaluated the environmental impacts of regional real-time pricing, similar specifications have been applied to renewable generation deployment (Callaway et al., 2018), electricity storage (Carson and Novan, 2013), electric vehicles (Graff Zivin et al., 2014), and natural gas price shocks related to fracking (Holladay and LaRiviere, 2017). However, this approach assumes the error term ε_{rt} is independently distributed after controlling for fixed effects. If emissions exhibit autoregressive or moving average dynamics, the model may suffer from omitted variable bias and inefficient parameter estimates.

²While the emission intensity of oil is comparable to coal, we exclude oil here. Oil-fired units function almost exclusively as super-peakers, meaning they are invariably the marginal fuel when active. The modeling challenge and focus of this study is distinguishing between gas and coal at the margin.

Hawkes (2010) proposed an alternative framework based on first-differencing:

$$\Delta E_t = \beta \Delta G_t + \varepsilon_t, \quad (2)$$

where $\Delta E_t = E_t - E_{t-1}$ measures the change in emissions between two consecutive hours, and $\Delta G_t = G_t - G_{t-1}$ denotes the corresponding change in electricity generation. Using Great Britain (GB) data (2002-2009), Hawkes (2010) estimated MEFs of approximately 690 kg CO₂/MWh, substantially exceeding the system AEF of 510 kg CO₂/MWh. Hawkes proposed differencing to interpret changes in the variables while, inadvertently, addressing the issue of non-stationary processes. Yet, as shown in Beltrami et al. (2020), standard tests most often fail to reject the hypothesis of stationarity. The evidence presented herein for the U.S., mirroring that of Europe (Beltrami et al., 2020, and Ben Amor et al., 2025), finds the relevant series to exhibit stationary properties. Therefore, Hawkes’ model does not represent, from a statistical perspective, the most parsimonious approach for estimating intra-day MEFs.

Indeed, Beltrami et al. (2020) shows that emissions and generation series for GB and Italy are stationary ($d = 0$). Consequently, their empirical specification simplifies to:

$$\Phi_p(L)(E_t - \beta G_t) = \alpha + \Theta_q(L)\varepsilon_t \quad (3)$$

with p and q selected via Akaike Information Criterion (AIC) and Bayesian Information Criterion (BIC), typically yielding ARIMA(1, 0, 1), ARIMA(2, 0, 1), or ARIMA(1, 0, 2) specifications. The authors demonstrate that the *ARIMA-FE* model consistently outperform both *US-FE* and *Hawkes* approaches according to information criteria. Crucially, their time series models generate more stable MEF trajectories with lower variance and coefficients of variation.

However, all three approaches rely on linear models that yield a single average marginal effect, invariant to the state of the system. We argue that this is ill-suited to the inherently non-linear nature of emissions and power generation. This motivates our use of MSMs, which allow the marginal emission factor to vary across latent regimes, thereby capturing the structural non-linearities that linear methods cannot accommodate.

3 Data sources and description

We construct our dataset using hourly electricity generation and emissions series for the lower 48 United States, obtained from Energy Information Administration (2026) (EIA), see Figure 1. The sample covers the period from 1 January 2019 to 31 December 2025, with a complete series of $T = 61,368$ hourly observations.

In line with relevant literature (Callaway et al., 2018, and Holland et al., 2022a), we rely on actual hourly generation rather than system load. Indeed, while load data is often used to approximate demand, it fails to account for the carbon intensity of imported electricity, e.g., cross-border flows from Canada or Mexico.

The aggregate CO₂ emissions E_t for each hour t can be represented as:

$$E_t = \sum_f G_{f,t} \cdot \theta_f \quad (4)$$

where $G_{f,t}$ denotes the hourly generation of fuel type f (i.e., coal or natural gas) and θ_f represents the respective emission factor.

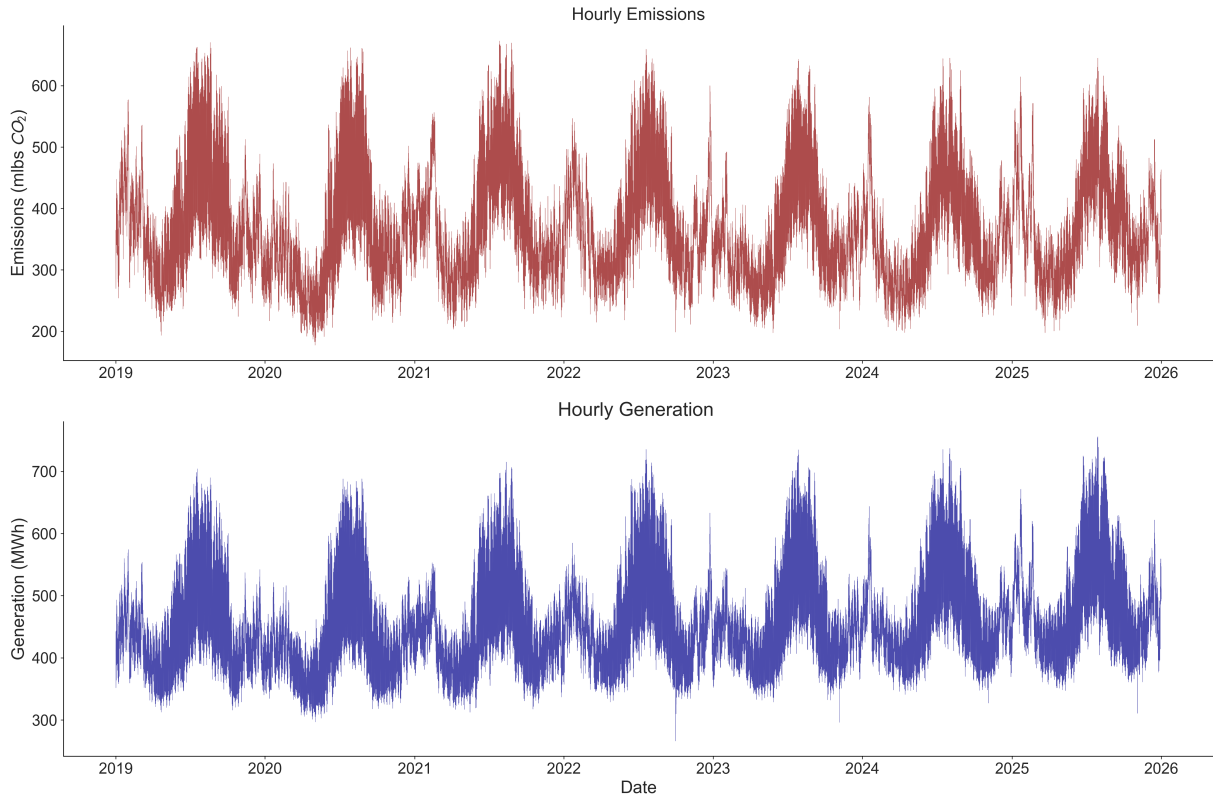


Figure 1: **Emissions and Generation:** Emissions are reported in Mlbs CO₂, while Generation in MWh refers to the total fossil fuel generation.

Table 1 presents the summary statistics for the full sample. The U.S. power system generated 461,092 MWh per hour, on average, and mean hourly emissions of approximately 168,050 lbs of CO₂. The high standard deviation in generation reflects the significant temporal heterogeneity of the grid.

Table 1: **Summary Statistics (2019–2025).**

Variable	N	Mean	Std. Dev.	Min	Max
Emissions (lbs)	61,368	168,050	41,036	80,496	305,224
Generation (MWh)	61,368	461,092	76,092	266,277	755,638

The dynamics are detailed in Table S1 of the Online Supplement (OS). Unlike many European systems that peak in winter (Beltrami et al., 2022), the U.S. is characterized by a dominant summer peak, driven by cooling demand. During summer months, mean generation surges to nearly 550,000 MWh, frequently forcing the dispatch of carbon-intensive peaker plants, which drives emissions to their annual maximums of about 219,000 lbs. The system reaches a trough during spring, where mild load and high renewable penetration reduce mean emissions to their minimum of 124,000 lbs.

3.1 Stochastic properties and empirical justification for Markov Switching Models

In this section, we examine the stochastic properties of CO₂ emissions to determine the appropriate modeling framework. Specifically, we verify whether the data, after controlling

for deterministic seasonality, exhibits stationarity while simultaneously possessing nonlinear characteristics.

To isolate the stochastic component, we first extracted the residuals from a linear regression that filters out deterministic seasonal effects using hourly, daily, and monthly indicators and a linear time trend. We then subjected these filtered residuals to a comprehensive battery of diagnostic tests, the results of which are summarized in Table 2.

Stationarity analysis

Table 2 (Panel A) reports the results of three complementary tests used to assess the presence of unit root and stationarity: the Augmented Dickey-Fuller (ADF), Phillips-Perron (PP), and Kwiatkowski-Phillips-Schmidt-Shin (KPSS) tests.

The lag lengths for the ADF test were selected via the BIC. The criterion consistently identified a range of 24–27 lags, capturing the physical 24-hour diurnal cycle of the power system. For the PP and KPSS tests, the spectral bandwidth was determined using the Newey-West estimator. We found a bandwidth between 37–55, ensuring robustness against the serial correlation and time-varying volatility inherent in high-frequency data.

The results show strong evidence of stationarity (see Panel A). Both the ADF and PP tests reject the null hypothesis of a unit root at the 1% significance level for every year in the sample, while the KPSS test fails to reject the null hypothesis of stationarity.

Nonlinearity and complexity

Having established stationarity, we investigated the residuals for nonlinear dependencies that standard linear models cannot capture. Panel B of Table 2 presents the results of Tsay’s F-test for nonlinearity, the BDS test for independence, and the Peña-Rodríguez (PR) test for volatility clustering.

To select the lag order p , we fitted a sequence of $AR(p)$ models to the residuals and selected the optimal order that minimized the AIC. We consistently found an optimal lag of $p = 11$ or 12 hours, reflecting the semi-diurnal operational cycles of the power system. Using this optimal lag, Tsay’s F-test strongly rejects the null of linearity ($p < 0.01$) for all years, indicating the presence of significant quadratic interactions. Furthermore, the BDS test statistics clearly rejects the hypothesis of independent and identically distributed (i.i.d.) noise. Crucially, the PR test strongly rejects the null of no autoregressive conditional heteroscedasticity (ARCH) effects, confirming the presence of volatility clustering.

These findings suggest that the underlying data generating process undergoes structural changes or regime shifts. This provides a robust empirical justification for adopting MSMs, which explicitly capture such regime-dependent dynamics.

4 Model specification and estimation methodology

We capture the dynamics of fossil fuel generation operating at the margin using a two-state MS-ARX. In this section, we define the model specification and detail the estimation procedure, which utilizes the expectation-maximization (EM) algorithm proposed by Dempster et al. (1977) and adapted for time series by Hamilton (1990). This iterative procedure integrates the (Hamilton, 1989) filter for forward inference and the (Kim, 1994) smoother for backward inference to facilitate maximum likelihood estimation (MLE).

Table 2: Diagnostic Tests for stationarity and nonlinearity. This table reports the test statistics for the emission residuals. **Panel A** reports stationarity tests: ADF, PP, and KPSS. **Panel B** reports nonlinearity tests: Tsay’s F-test, BDS test ($m = 6$), and PR test for volatility clustering.

Year	Panel A: Stationarity			Panel B: Nonlinearity		
	ADF	PP	KPSS	Tsay’s F	BDS	PR
2019	-8.22***	-8.66***	0.058	2.68***	198.72***	13.70***
2020	-8.79***	-9.71***	0.059	2.01***	203.59***	13.48***
2021	-8.24***	-8.59***	0.046	2.33***	219.82***	13.77***
2022	-8.95***	-8.45***	0.050	3.40***	220.18***	13.71***
2023	-8.50***	-9.40***	0.045	1.81***	197.40***	13.61***
2024	-8.02***	-8.69***	0.046	1.47***	203.75***	13.79***
2025	-7.70***	-8.23***	0.044	1.77***	197.91***	14.88***

***, **, and * indicate significance at the 1%, 5%, and 10% levels, respectively.

Note: For KPSS, a low statistic (no stars) indicates failure to reject stationarity.

4.1 Model specification

Let y_t denote the observed emission level at time t for $t = 1, \dots, T$, and $x_{1,t}$, $x_{2,t}$ for $t = 1, \dots, T$ the renewable and non-renewable³ generation covariates. The emissions process is governed by an unobserved discrete state variable $S_t \in \{1, 2\}$ ⁴. We interpret these regimes based on the fuel mix operating at the margin, namely we interpret a *Low-Emission state* if marginal generation is dominated by efficient natural gas units and *High-Emission state* if marginal generation shifts toward carbon-intensive coal or low-efficiency peaking units.

Conditional on the regime S_t , the observation equation is:

$$y_t = \alpha_{S_t} + \phi_{S_t} y_{t-1} + \beta_{1,S_t} x_{1,t} + \beta_{2,S_t} x_{2,t} + \epsilon_t, \quad \epsilon_t \sim \mathcal{N}(0, \sigma^2) \quad (5)$$

where ϕ_{S_t} is the autoregressive term, β_{1,S_t} is the *regime-specific* MEF, representing the marginal intensity of the grid in state S_t and β_{2,S_t} is the marginal probability of renewable sources in state S_t . The state variable S_t evolves according to a first-order ergodic Markov chain with transition matrix \mathbf{P} , where $p_{ij} = \mathbb{P}(S_t = j \mid S_{t-1} = i)$.

Although more general MSMs allowing for regime-dependent heteroscedasticity are widely used in the literature (Bauwens et al., 2010, and Kang, 2014), we impose a constant variance across regimes ($\sigma_1^2 = \sigma_2^2 = \sigma^2$) given theoretical and empirical considerations. Theoretically, this restriction ensures that regime identification is driven by structural shifts in merit order dispatch rather than transient volatility clustering. Indeed, regime-specific variances leads to weak identification of the mean parameters, as the likelihood tends to classify observations by volatility rather than by differences in marginal emissions (Hamilton and Susmel, 1994, and Sims et al., 2008). Empirically, we find that heteroscedastic Markov switching specifications systematically produce negative marginal emission factors in the low-emission regime, a physical impossibility that indicates model misspecification. This behavior arises because heteroscedastic MSMs tend to classify regimes primarily by variance rather than mean structure. In the electricity context, high-volatility periods (e.g., peak demand hours with rapid unit cycling) may coincide with either high or low

³In practice, we estimate non renewable generation as the sum of hourly generation from coal, gas provided in Energy Information Administration (2026).

⁴Although selection criteria suggest three states, an inspection of smoothed probabilities showed a third regime was redundant; thus, a two-state model was selected (see Section S2 of the Online Supplement for further details).

marginal emissions depending on the fuel mix. When the model partitions observations by volatility, the resulting mean parameters become biased, yielding negative coefficients that are empirically inconsistent with MEFs.

4.2 Likelihood and estimation strategy

The estimation of the parameter vector $\theta = (\beta_1, \beta_2, \sigma^2, p_{11}, p_{22})$ relies on MLE. However, because the state sequence $\mathcal{S} = (S_1, \dots, S_T)$ is unobserved, we cannot maximize the complete-data likelihood directly.

The quantity of interest is the *observed-data log-likelihood*, which marginalizes over all possible state sequences. Let \mathcal{Y}_T denote the full history of observations. The observed log-likelihood is:

$$\mathcal{L}_{obs}(\theta) = \sum_{t=1}^T \log f(y_t | \mathcal{Y}_{t-1}; \theta). \quad (6)$$

Direct maximization of (6) is computationally intractable because the marginal density $f(y_t | \dots)$ involves a summation over 2^T possible state paths.

To overcome this Hamilton (1990) developed a procedure which relies on the EM algorithm proposed by Dempster et al. (1977). Let us assume that a complete realization of the sequence $\mathcal{S} = (S_1, \dots, S_T)$ is known, it is possible to define the complete-data log-Likelihood as :

$$\mathcal{L}_c(\theta; \mathbf{y}, \mathcal{S}) = \sum_{t=1}^T \log f(y_t | S_t, \mathbf{x}_t; \theta) + \sum_{t=1}^T \log p_{S_{t-1}S_t}. \quad (7)$$

However, in practice the sequence $\mathcal{S} = (S_1, \dots, S_T)$ is unknown, so the role of the EM algorithm is to iteratively maximize the expected value of the complete-data log-likelihood (the Q-function) conditional on the observed data and the parameters from the previous iteration, $\theta^{(v)}$. In other words, the EM algorithm is divided into two steps: the (i) E-Step (Expectation) and the (ii) M-Step (Maximization).

The E-Step is where we compute the expectation of the log function given $\theta^{(v)}$ and \mathbf{y} :

$$Q(\theta | \theta^{(v)}) = \mathbb{E}_{S|\mathbf{y}, \theta^{(v)}} [\log L_c(\theta; \mathbf{y}, \mathcal{S})]. \quad (8)$$

This step requires computing the smoothed posterior probabilities of the regimes:

$$\xi_{t|T}^{(k)} = \mathbb{P}(S_t = k | \mathcal{Y}_T; \theta^{(v)}) \quad k = 1, 2 \quad (\text{Smoothed Probabilities}), \quad (9)$$

$$\xi_{t-1,t|T}^{(ij)} = \mathbb{P}(S_{t-1} = i, S_t = j | \mathcal{Y}_T; \theta^{(v)}) \quad (\text{Smoothed Joint Probabilities}). \quad (10)$$

The M-Step updates the parameters by finding the value that maximizes the expected complete-data log-likelihood:

$$\theta^{(v+1)} = \arg \max_{\theta} Q(\theta | \theta^{(v)}). \quad (11)$$

These steps are repeated until the increase in the observed likelihood (6) falls below a convergence tolerance. It has been shown that the EM algorithm converges to a local maximum (Dempster et al., 1977).⁵

⁵For further details on the Maximization step we refer the reader to Hamilton (1990).

5 Results and discussion

In this section, we present the findings of our Markov-Switching analysis applied to the US48 hourly emissions and generation data. We first validate the model specification, distinguishing our regime-switching approach from canonical linear benchmarks. Subsequently, we analyze the characteristics of the identified regimes and link their stability to the structural dynamics of the natural gas market.

5.1 Model comparison

The primary advantage of the MS-ARX framework over classical approaches, discussed in Section 2, is its ability to decompose the emission data generating process into distinct, mutually exclusive regimes. This allows for a time-varying estimation of MEFs that reflects the changing marginal fuel mix (i.e., coal vs. gas) rather than a static average.

A critical modeling decision in regime-switching frameworks is the selection of the autoregressive order (p). While preliminary diagnostics on the de-seasonalized emission series using Partial Autocorrelation Functions (PACF)⁶ suggested potential higher-order dependence, we performed a sensitivity analysis which reveals that increasing the lag order yields no substantial improvement in model fit while introducing severe instability. As reported in Table S4 of OS, estimating MS-ARX models with $p \geq 2$ consistently failed to converge across multiple optimization algorithms⁷. Furthermore, the marginal gains in likelihood for these unstable specifications were negligible, confirming that the additional complexity does not translate into meaningful improvements in explanatory power.

We therefore adopt a parsimonious MS-ARX(1) specification⁸. Conceptually, this imposes a clear division of labor: the AR(1) term captures short-run hour-to-hour persistence inherent in grid operations (e.g., thermal unit ramping constraints), while the regime-switching component absorbs slower-moving structural shifts in merit order (i.e., transitions from gas-driven to coal-driven states). Unlike the ARIMA specification, which smoothes over volatility, the regime-switching framework explicitly disentangles the distinct operating dynamics inherent to the merit-order dispatch. This structural identification allows quantification of how emissions vary across different fuel-margin states.

To assess the performance of our approach, we compared MS-ARX against the benchmarks defined in Section 2. To select the optimal orders of the ARIMA model, we apply an automated selection procedure based on MLE. The lag order p and the moving average order q are jointly chosen to maximize the log-likelihood of the model, while the integration order $d = 0$ because the series are stationary as shown in Section 3, leading to the best-fitting ARIMA(3,0,4) model.

A detailed comparison of model fit across ARIMA, MS-ARX and US-FE is reported in Table S5 of OS. The results reveal a clear ranking where ARIMA achieves the highest performance in terms of log-likelihood and lowest values across AIC, BIC, and Hannan-Quinn information criterion (HQIC), making it the best-fitting model, while MS-ARX places second. Both models exhibit a substantial gap relative to US-FE, reflecting the well-known limitations of linear models in capturing the nonlinear and persistent dynamics of the emissions. While MS-ARX does not achieve the best statistical fit compared to

⁶The plots of ACF and PACF for generation and emission are reported in Sections S3 and S4 of the Online Supplement

⁷This convergence failure is well-documented in the regime-switching literature (Hamilton, 1990, and Krolzig, 1997).

⁸Section S6 of the Online Supplement provides the residual diagnostics for MS-ARX(1).

ARIMA, its core value lies in the structural interpretation it provides. More precisely, MS-ARX captures state dependent behavior that neither ARIMA nor US-FE can offer, making it more suited to identifying different regimes of emissions driven by the merit-order dispatch.

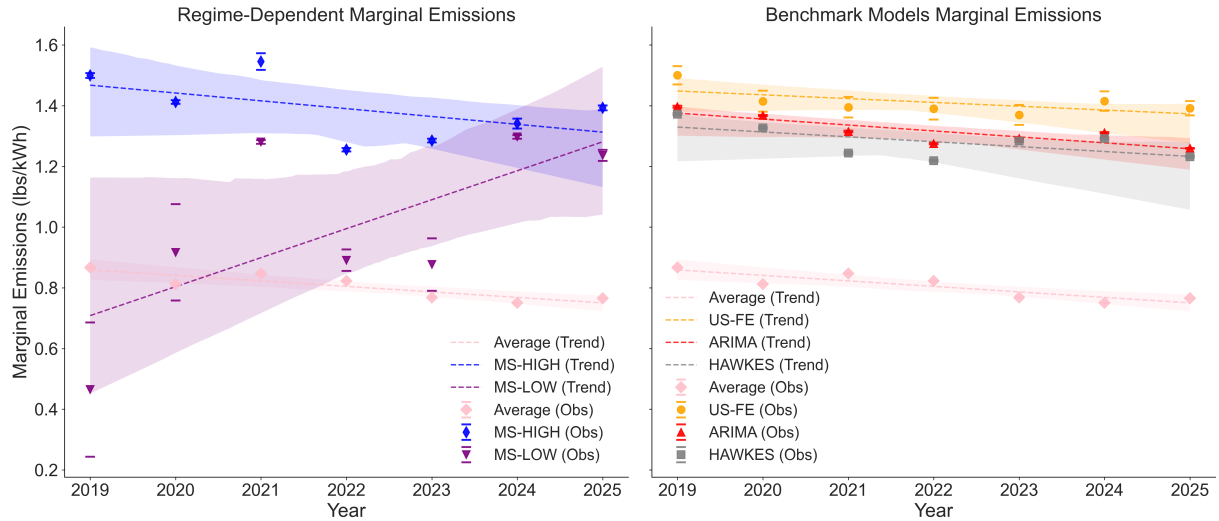


Figure 2: **Temporal evolution of MEFs (2019–2025).** (Left) **Regime-dependent dynamics:** The trajectories of the High-MEF and Low-MEF regimes. Note the convergence of the two states in the end of the considered period. (Right) **Benchmark Comparison:** Contrast between dynamic (ARIMA) and static (US-FE, HAWKES) linear specifications against the regime-switching baseline.

As illustrated in Figure 2, the distinct gap between average emissions (pink line) and all other models reaffirms that average emissions consistently underestimate marginal displacement potential. Moreover, in stark contrast to Holland et al. (2022a), our results show that for all methods we are comparing, MEFs follow a clear downward trend. Consistent with the discussion in Section 2, ARIMA-FE (red) provides a stable middle ground positioned between the US-FE (orange) and Hawkes (gray) estimates.

The *High-MEF* regime (blue) takes values close to those produced by the ARIMA, Hawkes, and US-FE estimates. This suggests that the this state captures the “dirty” marginal high fossil-fuel regime (i.e, predominantly coal). On the other hand, the *Low-MEF* regime (purple) yields smaller coefficients than the *High-MEF* regime, but exhibits greater volatility, particularly over the period 2019–2022. This divergence indicates that when the grid enters a “clean” fossil-fuel state, the marginal emission factor decouples from the linear aggregate trend.

By the end of the period, the two states converge. This alignment can be explained by the significant increase in the gas volume, driven by declining gas prices. As gas became cheaper, volumes increased, ultimately pushing the system toward a single dominant marginal source, in this case, gas. Standard linear models smooth over these episodes, masking the fact that during specific regimes, the marginal carbon benefit of an additional unit of generation is substantially lower than the annual average would suggest. Detailed coefficient estimates and standard errors for all models are reported in Table S6 of OS.

5.2 Temporal dynamics and drivers of regime switching

MSM frameworks not only have the advantage of revealing temporal MEF dynamics but also are able to disentangle distinct mutually exclusive MEF states. Figure 3 illustrates

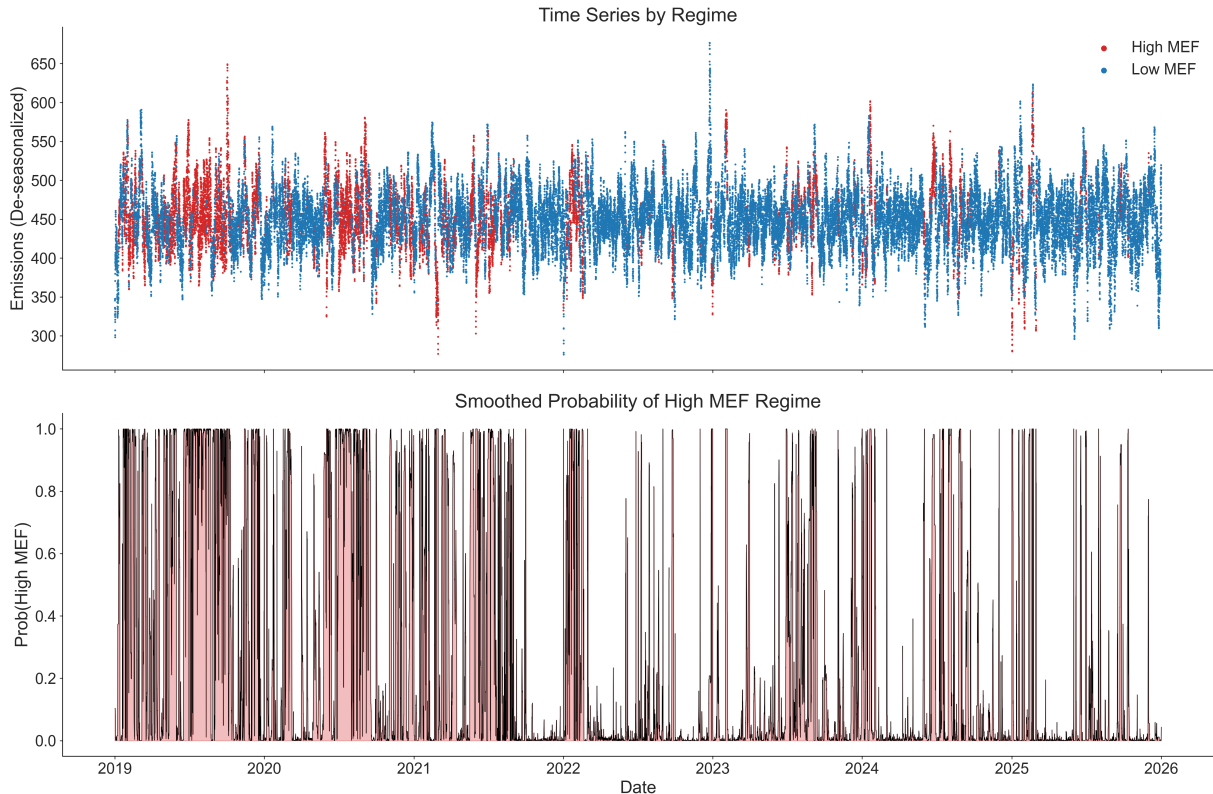


Figure 3: **Regime Switching Dynamics (2019–2025)**. Top: Hourly emissions colored by the most probable regime (Red = High MEF, Blue = Low MEF). Bottom: Smoothed probability $\mathbb{P}(S_t = \text{High MEF} | \mathcal{Y}_T)$. The distinct binary separation confirms that the grid operates in mutually exclusive states rather than a continuum.

this dichotomy, showing the time series of emissions by observed regime (top panel) and the smoothed probability of being in the *High-MEF* state (bottom panel).

Volatility and structural shifts

As evidenced by the smoothed probabilities, the *High-MEF* and *Low-MEF* regimes are rarely contemporaneous; the probability density is concentrated near 0 or 1, showing that at any given hour, the marginal technology is unambiguously defined.

However, the persistence of these regimes changes substantially over time. Prior to 2022, the system exhibits prolonged periods of stability where the *High-MEF* regime dominates. This behavior undergoes structural transformation coinciding with the last quarter of 2021, when the U.S. began experiencing heightened volatility in energy prices driven by a global energy crisis (we return to this in Section 5.3). Moreover, as shown in Figure 3 (bottom panel), the occurrence of the *High-MEF* state becomes less persistent and more volatile, characterized by rapid switching rather than sustained blocks.

Seasonality of marginal emissions

To further investigate the drivers of these regimes, Figure 4 decomposes the occurrence of *High-MEF* across seasonal and weekly cycles.

The *High-MEF* regime is not randomly distributed, but follows a clear load-driven pattern. Seasonally, it peaks during periods of cooling (summer) and heating (winter). During these peaks less efficient, carbon-intensive coal or oil peakers are dispatched to

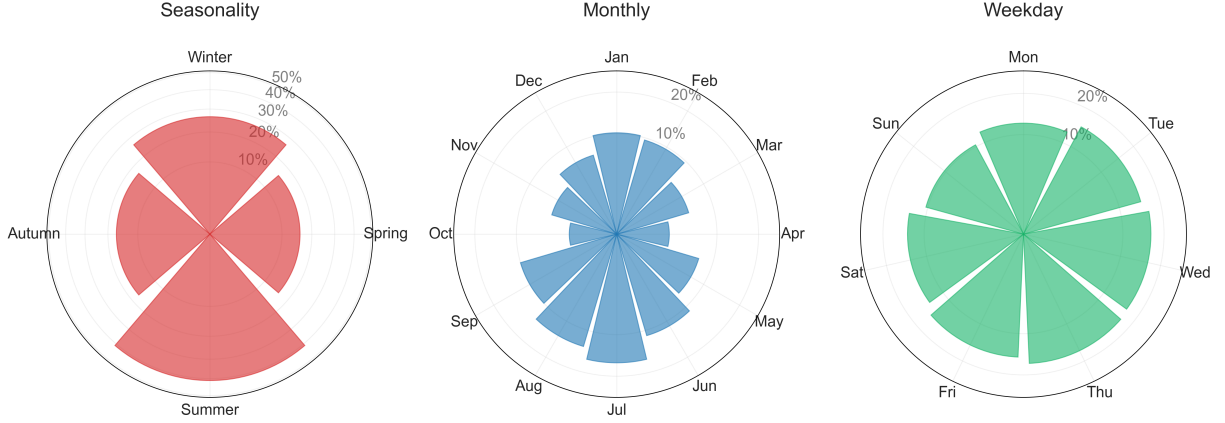


Figure 4: **Temporal Distribution of the High-MEF Regime.** Radial plots showing the percentage occurrence of the High-Emission state by Season (Left), Month (Center), and Day of Week (Right).

meet the marginal demand, thereby triggering the high-emission state. Conversely, the *High-MEF* probability contracts significantly during spring and autumn months, where mild demand allows cleaner gas units to set the price.

Identifying the marginal fuel

To unpack the physical behavior of the regimes, we investigate the marginal response of specific fuel technologies to system load fluctuations. We employ a first-difference linear specification to isolate the ramping behavior of marginal units from baseload generation. For each fuel type f and identified regime k , we estimate the following regression:

$$\Delta G_{f,t} = \alpha_f^{(k)} + \beta_f^{(k)} \Delta Load_t + \epsilon_{f,t} \quad \text{for } S_t = k \quad (12)$$

where Δ denotes the hourly change ($X_t - X_{t-1}$), $G_{f,t}$ is the generation of fuel f , and $Load_t$ represents the system demand.

The coefficient $\beta_f^{(k)}$ is defined as the *marginal fuel probability* (Holland et al., 2022a). It measures the proportion of an incremental megawatt (MW) of demand that is met by fuel f . Consequently, this value can be interpreted as the probability that a given fuel type is on the margin during regime k .

Figure 5 presents the estimated coefficients. There is a distinct shift in dispatch, whereby the *High-MEF* regime exhibits a higher probability of coal acting as the marginal fuel compared to the low regime.

5.3 Robust detection of structural break in natural gas markets

To identify the exogenous drivers of the observed regime instability, we draw on the insights of Holladay and LaRiviere (2017) and Knittel et al. (2015). These studies demonstrate that structural breaks and changes in fuel prices can fundamentally alter MEFs by shifting the dispatch order of power plants. When natural gas is expensive, it is typically reserved for peaking capacity during high-demand periods, while relatively inexpensive coal serves as the baseload. However, as gas prices fall, efficient natural gas plants become cheaper to operate, displacing coal from the baseload and pushing it to the margin, where it sets a higher marginal emission rate for the system (Holland et al., 2022a).

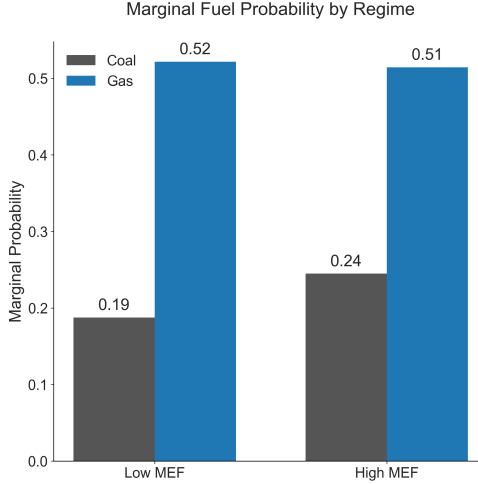


Figure 5: **Marginal Fuel Probability by Regime.** The bar chart displays the estimated β coefficients from Equation (12). It illustrates that Gas is the dominant marginal fuel in the Low MEF regime, while Coal significantly increases its marginal contribution in the High MEF regime.

To analyze this shift, we examine daily Henry Hub natural gas spot prices⁹. Indeed, natural gas prices exhibit marked volatility and frequent spikes (see Figure 6); this behavior is documented in the electricity market by Gianfreda and Grossi (2012) and Grossi and Nan (2019). Although different procedures to detect instability are widely used in the electricity and financial markets (Apergis and Lau, 2015, and Vriz and Grossi, 2026), many of them are highly sensitive to outliers and transient shocks. Given this susceptibility to extreme events, we adopt the robust monitoring approach proposed by Rousseeuw et al. (2019) to detect a structural break in slope.

Detecting Structural break

We model the daily natural gas price P_t as a trend-stationary process subject to a potential regime change at an unknown time τ . Specifically, we test for a structural break in the slope of the price trend, allowing us to distinguish between a stable long-term trajectory and the onset of a new pricing regime. The robust broken-trend model is specified as follows:

$$P_t = \alpha + f(t) + \delta(t - \tau)I(t > \tau) + \epsilon_t, \quad t = 1, \dots, T \quad (13)$$

where α is the intercept, $f(t)$ represents the non linear baseline price trend, and δ denotes the slope change that occurs after the break date τ . The term $I(\cdot)$ is the indicator function, taking the value of 1 if $t > \tau$ and 0 otherwise. The error term ϵ_t is assumed to be independent, but may follow a heavy-tailed distribution contaminated by outliers.

Robust Estimation Strategy

To estimate the unknown breakpoint τ robustly, we minimize the trimmed sum of squared residuals rather than the total sum of squares. Following Rousseeuw et al. (2019), we define the trimmed objective function $S(\tau)$ as:

⁹Data have been downloaded by U.S. Energy Information Administration (2026).

$$S(\tau) = \sum_{j=1}^h (r^2)_{(j)}(\tau) \quad (14)$$

where $(r^2)_{(1)}(\tau) \leq (r^2)_{(2)}(\tau) \leq \dots \leq (r^2)_{(T)}(\tau)$ are the ordered squared residuals from the model estimated conditional on break date τ . The trimming parameter h represents the number of smaller squared residuals used for estimation. We set $h = 0.99T$, thereby effectively ignoring the 1% most extreme observations during the search procedure to prevent masking effects.

The estimated break date $\hat{\tau}$ is the solution to the discrete optimization problem:

$$\hat{\tau} = \arg \min_{\tau \in \Gamma} S(\tau) \quad (15)$$

where $\Gamma = [[0.15T], [0.85T]]$ is the search window, trimmed at the boundaries to ensure parameter stability (Andrews, 1993).

Inference and Outlier Detection

Since the asymptotic distribution of the raw LTS estimator is non-standard, we employ a reweighting procedure to perform valid statistical inference on the slope change parameter δ (Rousseeuw and Hubert, 2018).

First, we calculate a robust scale estimate $\tilde{\sigma}$ based on the minimized trimmed loss, adjusted for consistency with the normal distribution (Croux and Rousseeuw, 1992):

$$\tilde{\sigma} = c_{h,T} \sqrt{\frac{S(\hat{\tau})}{h}} \quad (16)$$

where $c_{h,T}$ is a consistency factor correcting for the truncation of the error distribution ¹⁰. Using this scale, we identify outliers by computing standardized residuals. An observation P_t is assigned a weight w_t :

$$w_t = \begin{cases} 1 & \text{if } |r_t(\hat{\tau})/\tilde{\sigma}| \leq \Phi^{-1}(0.995) \\ 0 & \text{otherwise} \end{cases} \quad (17)$$

Finally, we estimate the model in Equation (13) using weighted least squares. The statistical significance of the structural break is determined by the t -statistic of the estimate \hat{t}_δ . We reject the null hypothesis of a stable trend if $|\hat{t}_\delta| > 1.96$, confirming a structural break candidate robust to distributional anomalies.

Timing and magnitude of the shock

Figure 6 reports the results of the robust monitoring procedure. The estimated break date $\hat{\tau}$, identified as the minimiser of Equation (15) falls on May 31, 2022.

This break point effectively partitions the sample into two distinct economic phases: the *Inflationary Phase (2019–May 2022)*, characterized by rising fuel costs, driven by post-pandemic demand recovery and heightened geopolitical tensions, and the *Correction Phase (Post-May 2022)*, where prices retreat from their highs, stabilizing at a lower mean level, albeit with continued volatility.

¹⁰Asymptotically, it is defined as $c_{h,T} = \sqrt{\frac{1}{1 - \frac{2n}{h} q \phi(q)}}$, where $q = \Phi^{-1}\left(\frac{h+n}{2n}\right)$ is the quantile of the standard normal distribution corresponding to the trimming proportion, and $\phi(\cdot)$ and $\Phi(\cdot)$ denote the standard normal density and cumulative distribution functions, respectively (Rousseeuw and Leroy, 1987).

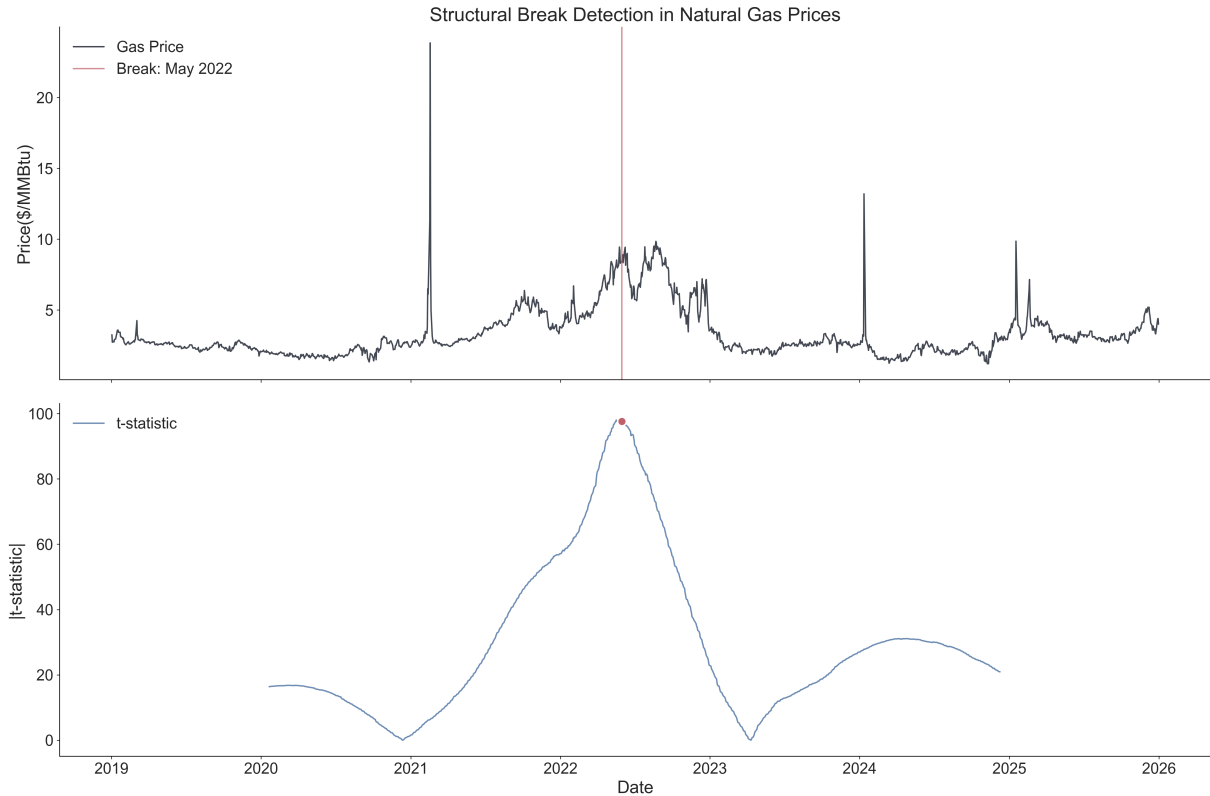


Figure 6: **Robust detection of structural break in gas prices.** Top panel: Daily natural gas spot prices with the estimated break date (May 31, 2022) marked by the vertical line. Bottom panel: The sequence of robust t-statistics for the slope change parameter (δ).

Link to merit order dynamics

The timing of this structural break offers a possible explanation for the regime switching behavior observed in Section 5.2. Prior to the break (2021–early 2022), the sustained rise in gas prices eroded the competitive advantage of natural gas combined cycle (NGCC) units, frequently pushing them out of the baseload and allowing coal to set the marginal price. This aligns with the “stable blocks” of High-MEF regimes observed in Figure 3.

Conversely, the negative trend post-May 2022 restored the economic competitiveness of gas. As prices fell, gas units regained their position in the merit order. However, the market did not return to a simple stable state; rather, it entered a period of volatility where the *High-MEF* (coal-driven) regime appears intermittently at the margin.

5.4 Impact of structural break on daily MEF profiles

To investigate how the May 2022 structural break altered the carbon intensity of the grid at the hourly level, we re-estimated the Markov Switching coefficients for two distinct sub-periods: the *Inflationary phase* (2019–May 2022) and the *Correction phase* (Post-May 2022).

Figure 7 contrasts the hourly profiles of the *Low-MEF* and *High-MEF* regimes across these two phases. The results¹¹ reveal a systemic reduction in marginal emissions in both states. In the *Low-MEF* state (left panel), the post-break curve (dashed) lies below the pre-break baseline. The overnight and early morning hours show a moderate decline

¹¹The values for the MEFs, SE, and average load are provided in Table S7 of the Online Supplement.

with respect to pre-break however, during the afternoon and evening, MEFs drop sharply, reaching values as low as 1.076 at hour 19. The low regime after the break is therefore telling a story of a grid that is on average cleaner at the margin but considerably more variable, especially in hours where renewable intermittency is more pronounced.

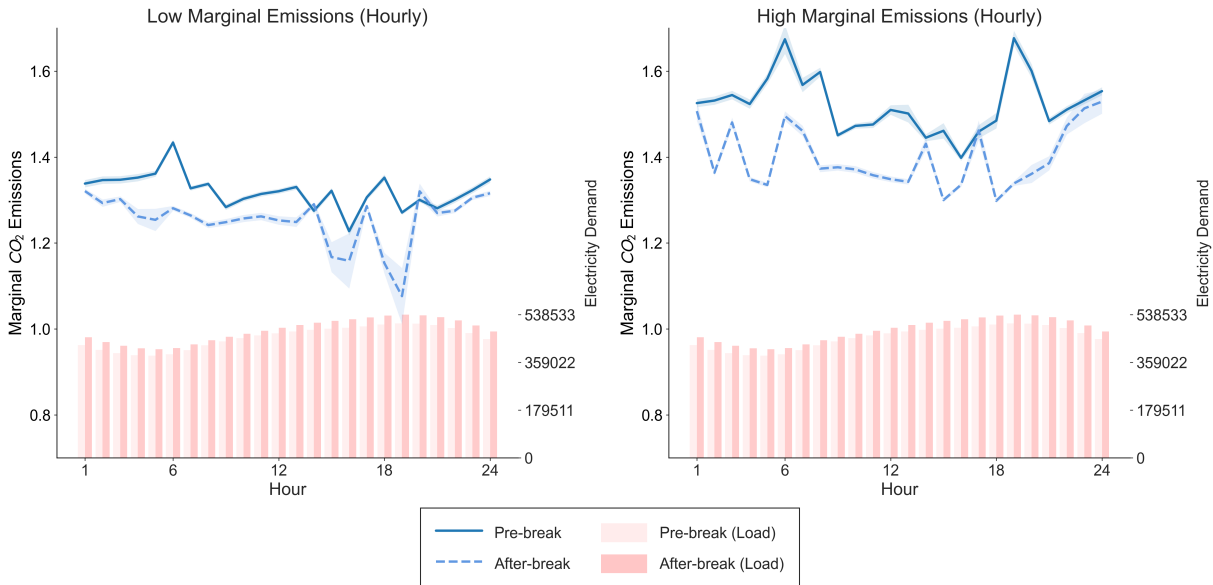


Figure 7: **Structural Shift in Diurnal Marginal Emissions (2019–2025)**. Comparison of hourly MEFs for the pre-break (2019–2021, solid blue) and post-break (2022–2025, dashed light blue) periods. The left panel shows the Low-Emission regime, while the right panel displays the High-Emission regime. The pink bars represent the average hourly load profile.

The clearest impact of the structural break, however, is observed in the *High-MEF* regime (right panel). Historically (pre-break), this regime was characterized by MEFs exceeding 1.6 lbs/kWh. Yet, in the post-break phase, emissions of this state fell by around 0.1–0.2 lbs/kWh across the day. This suggests that the decline in gas prices discussed in Section 5.3 pushed coal out of the merit order even during stressed grid conditions.

5.5 Understanding the mechanisms affecting marginal emission factors

To disentangle the drivers of MEFs in the US48 region, we examine the evolution of the generation mix through two distinct lenses: *average generation* (the volume of fuel consumed) and *marginal responsiveness* (the probability that a specific fuel meets the next unit of demand). While the share of coal in baseload generation has historically declined, marginal emissions may increase or decrease depending on whether coal or gas becomes the primary marginal source (Knittel et al., 2015, and Holland et al., 2022a).

Econometric estimation of marginal responsiveness

Our statistical approach for examining this structural shift adapts the methodology established by Holland et al. (2022a) for estimating marginal emissions. We estimate the responsiveness of coal and gas to changes in system load using the following linear regression model for each year y :

$$Gen_{f,t} = \beta_{f,y} \cdot Load_t + \alpha_{m,h} + \epsilon_t \quad (18)$$

where $Gen_{f,t}$ is the hourly aggregate generation from fuel source f at hour t , $Load_t$ is the hourly system-wide electricity demand, $\alpha_{m,h}$ represents *month-of-sample* by *hour-of-day* fixed effects. This term absorbs predictable variation due to seasonality and daily schedules, ensuring that the estimate is driven by stochastic deviations in load rather than predictable cycles. $\beta_{f,y}$ is the coefficient of interest, representing the marginal response rate, which can be interpreted as the probability that the marginal unit of load is met by generation from fuel source f .

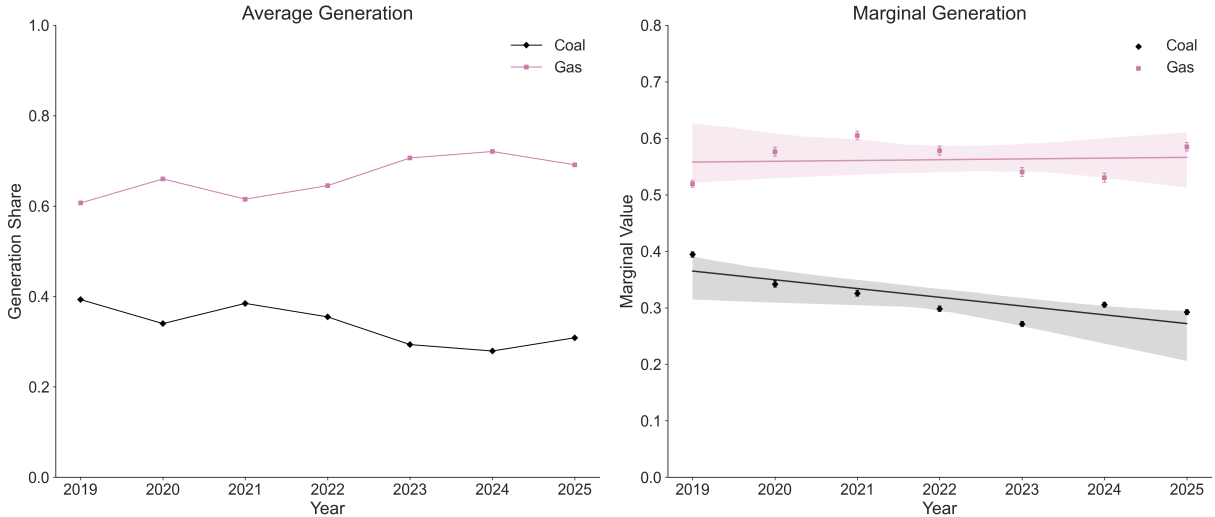


Figure 8: **Fuel Mix Evolution.** Comparison of average generation shares (Left) and marginal responsiveness (Right) for coal and gas. The data reveal a structural shift as coal’s marginal role diminishes significantly over the considered period.

Figure 8 illustrates the evolution of the fuel mix dynamics over the considered period. The left panel displays the average generation share for coal and gas, while the right panel reports their marginal responsiveness.

As shown in the left panel, the spread between gas and coal shares was relatively narrow in 2021. However, this gap has widened significantly in subsequent years, establishing gas as the dominant source on average. A similar divergence is observed in the right panel regarding marginal responsiveness: while the probability of gas being at margin slightly increased, the marginal role of coal has decreased sharply. The distinction between a coal-driven and gas-driven regime is therefore fading, as the system is effectively collapsing toward a single regime dominated by gas in both average and marginal emissions.

5.6 MEF regimes and the energy crisis

Finally, we investigate the impact of the structural break on marginal emission regimes using an interaction with an indicator variable equal to 1 if May 2022 or later and 0 otherwise. The appropriate Markov-switching specification can be obtained by modifying Equation(5) in the following way:

$$y_t = \alpha_{s_t} + x_t^T \beta_{s_t} + (D_t \times x_t)^T \delta_{s_t} + \varepsilon_t, \quad \varepsilon_t \sim \mathcal{N}(0, \sigma^2), \quad (19)$$

where $x_t = [x_{1,t}, x_{2,t}]$ and D_t represents the post-2022 indicator that captures a structural change in marginal emissions. The implied marginal emission factors can be interpreted as β_{s_t} for the after break period and $\beta_{s_t} + \delta_{s_t}$ for the post-break period where δ_{s_t} accounts for the post-crisis change in marginal emissions within each regime.

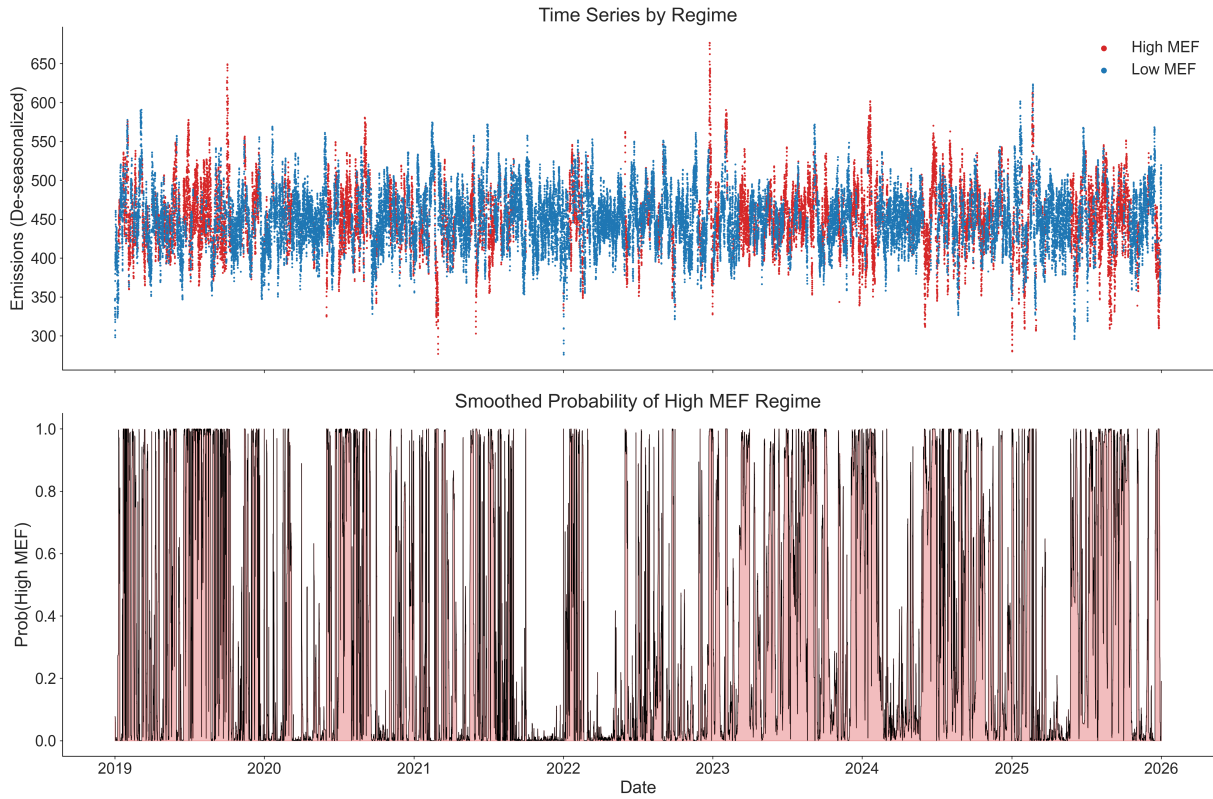


Figure 9: **Regime Switching Dynamics for dummy model (2019–2025)**. Top: Hourly emissions colored by the most probable regime (Red = High MEF, Blue = Low MEF). Bottom: Smoothed probability $\mathbb{P}(S_t = \text{High MEF} | \mathcal{Y}_T)$.

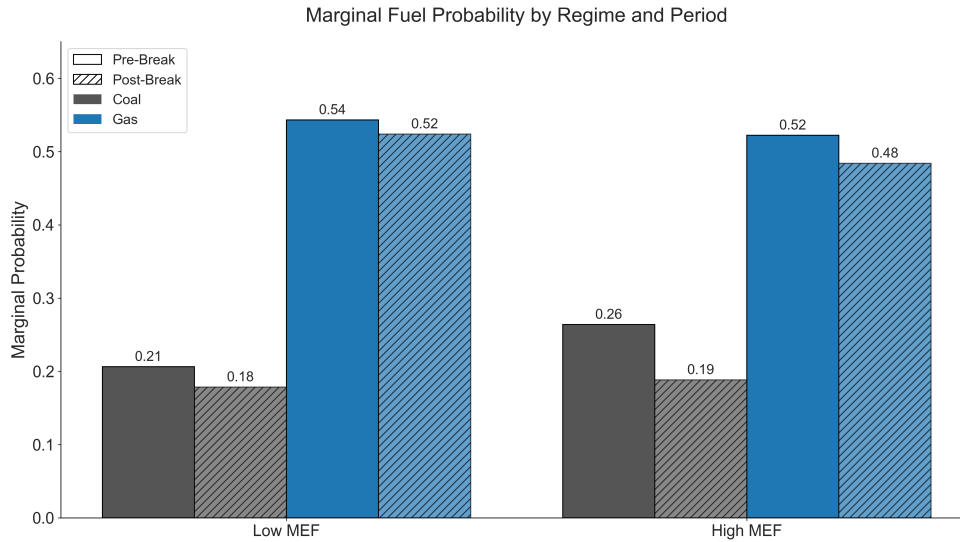


Figure 10: **Marginal Fuel Probability by Regime and Period**. The bar chart displays the estimated β coefficients from Equation (12) for the Pre-Break (2019–May 2022) and Post-Break (Post-May 2022) periods. While Gas remains the dominant marginal source across both states, the Post-Break period shows a marked convergence where the marginal responsiveness of coal becomes nearly indistinguishable between regimes, signaling a system increasingly dominated by natural gas.

The results¹² show that the interaction terms δ_{s_t} are negative and statistically significant

¹²Table S8 of the Online Supplement provides the coefficients and SEs of the models estimated by Equations (5) and (19).

in both post-break regimes and the transition probabilities in the model with the interaction terms no longer display the same pattern observed in the baseline model without the event indicator. This transition induced lasting changes in the generation mix and dispatch order. Even as gas prices declined, the marginal emissions response to load remained structurally altered relative to the pre-crisis period. These features clearly feature in the regime dynamics and marginal fuel probabilities in Figures 9 and 10, respectively.

6 Conclusion

This study uncovers the existence of MEF regimes in the U.S. power sector. By employing MS-ARX, we show that canonical linear models hide important dynamics, notably the evolution of distinct “low” and “high” fossil-fuel regimes and their apparent convergence over time. We augment the analysis by identifying a structural break at the height of the global energy crisis (May 2022). Accounting for this gas price shock reveals a common structural shift within existing regimes rather than the emergence of a new state.

Our approach is also novel in that, upon controlling for multiple regimes and structural breaks, we are able to explain why MEFs are now trending *downward*, counter to the increasing trend in 2010–2019 reported by [Holland et al. \(2022a\)](#). These findings suggest that executive orders designed to subvert the scheduled retirement of coal-fired plants to meet growing demand may only serve to exert upward pressure on both emissions and prices at the margin.

Data Availability Statement

The data supporting the findings of this study are publicly available. Hourly electricity generation and emissions data were sourced from [Energy Information Administration \(2026\)](#), and natural gas pricing data were obtained from the EIA Henry Hub spot price index ([U.S. Energy Information Administration, 2026](#)). To ensure scientific transparency and reproducibility, the complete processing pipeline, model implementation, and source code are available at the following GitHub repository: [STATE_DEPENDENT_MEF](#).

References

- Andrews, D. W. (1993). Tests for parameter instability and structural change with unknown change point. *Econometrica*, 61(4):821–856.
- Apergis, N. and Lau, M. C. K. (2015). Structural breaks and electricity prices: Further evidence on the role of climate policy uncertainties in the Australian electricity market. *Energy Economics*, 52:176–182.
- Bauwens, L., Preminger, A., and Rombouts, J. V. K. (2010). Theory and inference for a Markov switching GARCH model. *The Econometrics Journal*, 13(2):218–244.
- Beltrami, F., Burlinson, A., Giulietti, M., Grossi, L., Rowley, P., and Wilson, G. (2020). Where did the time (series) go? Estimation of marginal emission factors with autoregressive components. *Energy Economics*, 91:104905.
- Beltrami, F., Fontini, F., Giulietti, M., and Grossi, L. (2022). The zonal and seasonal CO₂ marginal emissions factors for the Italian power market. *Environmental and Resource Economics*, 83(2):381–411.
- Ben Amor, S., Sgarciu, S., BatzLineiro, T., and Muesgens, F. (2025). Advanced models for hourly marginal CO₂ emission factor estimation: A synergy between fundamental and statistical approaches. *Applied Energy*, 397:126265.
- Callaway, D., Fowle, M., and McCormick, G. (2018). Location, location, location: The variable value of renewable energy and demand-side efficiency resources. *Journal of the Association of Environmental and Resource Economists*, 5(1):39–75.
- Carson, R. T. and Novan, K. (2013). The private and social economics of bulk electricity storage. *Journal of Environmental Economics and Management*, 66(3):404–423.
- Croux, C. and Rousseeuw, P. J. (1992). Time-efficient algorithms for two highly robust estimators of scale. In *Computational Statistics*, pages 411–428. Physica-Verlag HD.
- Dempster, A. P., Laird, N. M., and Rubin, D. B. (1977). Maximum likelihood from incomplete data via the EM algorithm. *Journal of the Royal Statistical Society: Series B (Methodological)*, 39(1):1–38.
- Energy Information Administration (2026). Hourly CO₂ emissions estimates.
- Gagnon, P. J., Bistline, J. E. T., Alexander, M. H., and Cole, W. J. (2022). Short-run marginal emission rates omit important impacts of electric-sector interventions. *Proceedings of the National Academy of Sciences*, 119(49):e2211624119.
- Gianfreda, A. and Grossi, L. (2012). Forecasting Italian electricity zonal prices with exogenous variables. *Energy Economics*, 34(6):2228–2239.
- Graff Zivin, J., Kotchen, M., and Mansur, E. (2014). Spatial and temporal heterogeneity of marginal emissions: Implications for electric cars and other electricity-shifting policies. *Journal of Economic Behavior and Organization*, 107:248–268.
- Grossi, L. and Nan, F. (2019). Robust forecasting of electricity prices: Simulations, models and the impact of renewable sources. *Technological Forecasting and Social Change*, 141:305–318.

- Hamilton, J. (1989). A new approach to the economic analysis of nonstationary time series and the business cycle. *Econometrica*, 57(2):357–384.
- Hamilton, J. D. (1990). Analysis of time series subject to changes in regime. *Journal of Econometrics*, 45(1-2):39–70.
- Hamilton, J. D. and Susmel, R. (1994). Autoregressive conditional heteroskedasticity and changes in regime. *Journal of Econometrics*, 64(1):307–333.
- Hawkes, A. D. (2010). Estimating marginal CO2 emissions rates for national electricity systems. *Energy Policy*, 38(10):5977–5987.
- Holladay, J. S. and LaRiviere, J. (2017). The impact of cheap natural gas on marginal emissions from electricity generation and implications for energy policy. *Journal of Environmental Economics and Management*, 85:205–227.
- Holland, S., Kotchen, M., Mansur, E., and Yates, A. (2022a). Why marginal CO2 emissions are not decreasing for US electricity: Estimates and implications for climate policy. *Proceedings of the National Academy of Sciences*, 119(8):e2116632119.
- Holland, S. P., Kotchen, M. J., Mansur, E. T., and Yates, A. J. (2022b). Reply to Gagnon et al.: Short-run estimates vs. long-run conjectures. *Proceedings of the National Academy of Sciences*, 119(49):e2214219119.
- Holland, S. P. and Mansur, E. T. (2008). Is real-time pricing green? The environmental impacts of electricity demand variance. *The Review of Economics and Statistics*, 90(3):550–561.
- Kang, K. H. (2014). Estimation of state-space models with endogenous Markov regime-switching parameters. *The Econometrics Journal*, 17(1):56–82.
- Kapoor, G., Wichitaksorn, N., and Zhang, W. (2023). Analyzing and forecasting electricity price using regime-switching models: The case of new zealand market. *Journal of Forecasting*, 42(8):2011–2026.
- Kim, C.-J. (1994). Dynamic linear models with Markov-Switching. *Journal of Econometrics*, 60(1-2):1–22.
- Knittel, C. R., Metaxoglou, K., and Trindade, A. (2015). Natural gas prices and coal displacement: Evidence from electricity markets. Working Paper 21627, NBER.
- Koster, P. and Mosler, K. (2006). Can Markov regime-switching models improve power-price forecasts? Evidence from German daily power prices. *Applied Energy*, 83:943–958.
- Krolzig, H. (1997). *Markov-Switching Vector Autoregressions: Modelling, Statistical Inference, and Application to Business Cycle Analysis*. Springer.
- Rousseeuw, P. J. and Hubert, M. (2018). Anomaly detection by robust statistics. *Wiley Interdisciplinary Reviews: Data Mining and Knowledge Discovery*, 8(2):e1236.
- Rousseeuw, P. J. and Leroy, A. M. (1987). *Robust Regression and Outlier Detection*. John Wiley & Sons, New York.

- Rousseuw, P. J., Perrotta, D., Riani, M., and Hubert, M. (2019). Robust monitoring of time series with application to fraud detection. *Econometrics and Statistics*, 9:108–121.
- Sims, C. A., Waggoner, D. F., and Zha, T. (2008). Methods for inference in large multiple-equation Markov-switching models. *Journal of Econometrics*, 146(2):255–274.
- U.S. Department of Energy (2023). On the path to 100% clean electricity. Report, U.S. Department of Energy, Washington, D.C.
- U.S. Department of State (2021). Pathways to net-zero greenhouse gas emissions by 2050. Report, U.S. Department of State, Washington, D.C.
- U.S. Energy Information Administration (2026). Henry Hub Natural Gas Spot Price (dollars per Million Btu). Accessed: 2026-02-26.
- U.S. Environmental Protection Agency (2019). Inventory of U.S. greenhouse gas emissions and sinks.
- Vriz, G. L. and Grossi, L. (2026). Green bubbles: A four-stage paradigm for detection and propagation. *Energy Economics*, 154:109095.
- Zachmann, G. (2007). A Markov switching model of the merit order to compare british and german price formation. *DIW Discussion Papers No. 714*.

Supplementary Material

S1 Summary Statistics

Table S1: **Summary Statistics by Season.** This table reports the mean, standard deviation, minimum, and maximum values for Hourly Emissions (lbs) and Generation (MWh) across different seasons from 2019 to 2025.

Season	Hourly Emissions (lbs)				Hourly Generation (MWh)			
	Mean	Std	Min	Max	Mean	Std	Min	Max
<i>Spring</i>								
2019	153,120	28,093	87,727	243,056	415,025	49,534	312,704	566,117
2020	124,767	21,065	80,496	199,931	383,655	41,681	296,842	532,255
2021	139,810	21,836	92,283	221,124	401,748	43,360	312,529	575,181
2022	144,154	20,899	97,387	232,358	422,801	46,712	329,023	627,329
2023	133,167	19,278	89,607	192,238	418,630	40,764	328,878	558,459
2024	128,306	19,514	89,758	193,940	430,736	45,697	341,008	591,933
2025	133,520	17,951	89,692	189,301	437,081	42,303	347,238	579,171
<i>Summer</i>								
2019	208,306	47,045	107,182	304,093	510,028	86,082	345,647	704,164
2020	202,905	48,252	93,482	300,184	507,714	88,469	324,232	687,997
2021	219,163	39,930	122,107	305,224	519,315	84,681	333,228	715,022
2022	210,816	39,168	115,397	299,069	533,204	86,482	347,843	735,343
2023	200,827	40,388	111,557	291,720	531,102	86,576	350,066	734,735
2024	200,108	39,262	107,060	292,553	547,909	83,441	362,731	737,011
2025	202,693	36,899	112,535	292,512	554,873	87,809	360,166	755,638
<i>Autumn</i>								
2019	173,055	36,348	101,654	280,125	438,322	66,274	315,900	653,035
2020	154,824	30,538	97,085	265,489	415,751	56,014	317,800	633,456
2021	161,059	30,573	103,764	261,606	431,537	58,133	317,510	624,411
2022	157,974	30,052	90,132	263,658	435,311	60,365	266,277	642,757
2023	155,580	29,078	92,352	273,187	444,760	61,597	296,158	697,800
2024	151,882	26,538	101,477	234,034	449,898	56,112	327,225	622,791
2025	159,825	25,947	94,952	242,684	463,077	58,036	310,793	629,455
<i>Winter</i>								
2019/20	153,481	22,742	98,422	221,682	424,921	37,425	334,553	542,145
2020/21	180,941	26,648	112,598	252,382	454,154	38,307	343,078	553,033
2021/22	170,805	29,296	101,161	248,005	457,730	41,679	336,901	584,792
2022/23	161,609	29,076	108,197	272,148	457,206	43,077	352,285	632,995
2023/24	162,237	30,886	99,372	263,728	463,787	44,530	364,881	643,682
2024/25	179,923	32,059	106,155	278,738	492,871	50,514	369,560	671,200

S2 Selection of the Number of Regimes

To determine the optimal number of latent regimes (k) for the Markov Switching Model (MSM), we estimated specifications for $k = 2$ and $k = 3$ under $p = 1$ using the full sample period (2019–2025). The model selection criteria are presented in Table S2.

Table S2: **Model fit statistics for Markov Switching specifications.** Comparison of log-likelihood and information criteria for 2-state and 3-state specifications.

States (k)	Log-Likelihood	AIC	BIC	HQIC
2	111,455.35	-222,888.69	-222,789.42	-222,857.89
3	112,419.08	-224,800.17	-224,628.70	-224,746.96

Note: AIC = Akaike Information Criterion; BIC = Bayesian Information Criterion; HQIC = Hannan-Quinn Information Criterion. All models achieved convergence. The 3-state specification provides a 0.86% improvement in Log-Likelihood relative to the 2-state model.

Justification for Model Selection:

While the information criteria (AIC, BIC, and HQIC) are minimized for the 3-state specification, statistical fit must be weighed against economic interpretability and regime persistence. A post-estimation diagnostic of the smoothed probabilities (reported in Table S3) revealed that the 3-state model is over-specified.

Specifically, the regime identified as ‘Regime 1’ captured only 0.8% of the sample observations. In a Markov Switching framework, a state with such negligible probability mass (frequency < 1%) does not represent a persistent market structure but rather captures transient anomalies or outliers.

Consequently, we rejected the 3-state model in favor of the parsimonious 2-state specification, which identifies two robust, persistent regimes that align with the physical merit order.

Table S3: **Regime Frequency Diagnostics (3-State Model).** The extremely low frequency of Regime 1 indicates model over-specification.

Regime	Frequency (%)	Classification Status
Regime 0	74.9%	Valid
Regime 1	0.8%	Rejected (Transient/Outlier)
Regime 2	24.3%	Valid

Note: Frequency is defined as the percentage of hours where the smoothed probability of the regime exceeds that of all other regimes ($P(S_t = k|I_T) > P(S_t \neq k|I_T)$).

S3 Emissions Diagnostics (2019–2025)

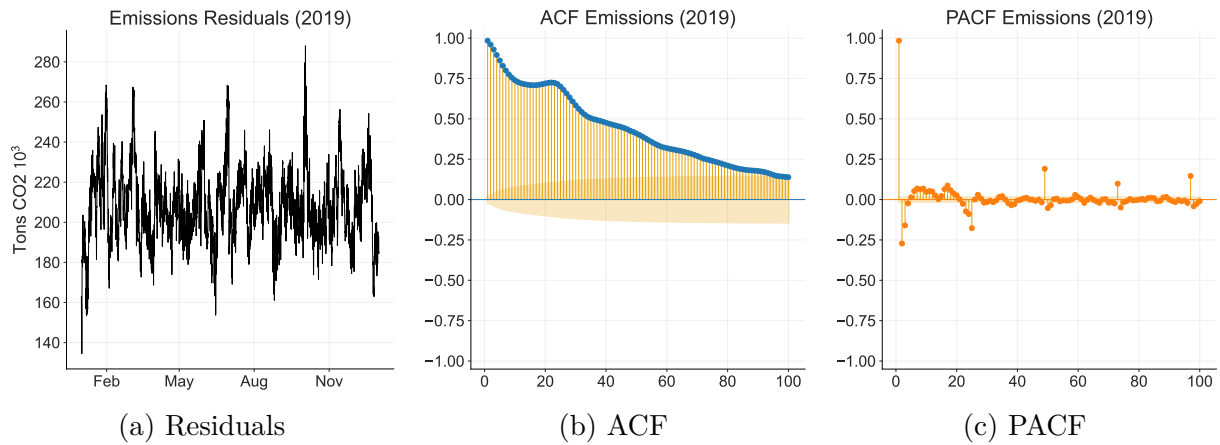


Figure S1: Diagnostic plots for **Emissions** (2019).

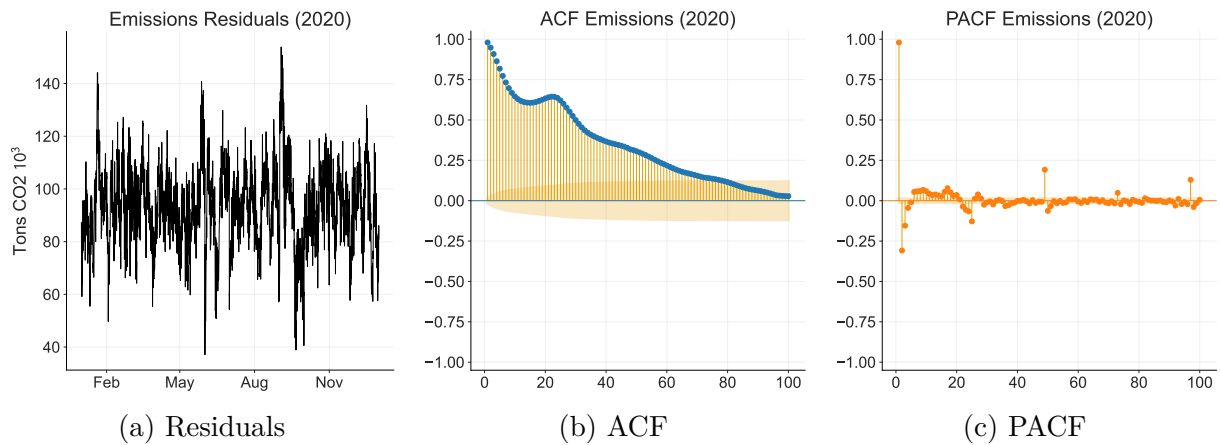


Figure S2: Diagnostic plots for **Emissions** (2020).

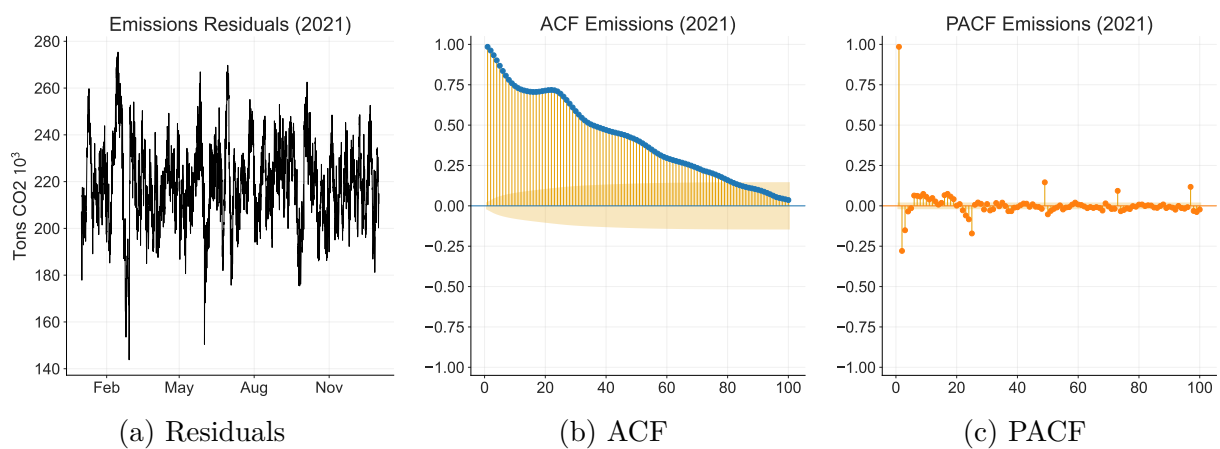


Figure S3: Diagnostic plots for **Emissions** (2021).

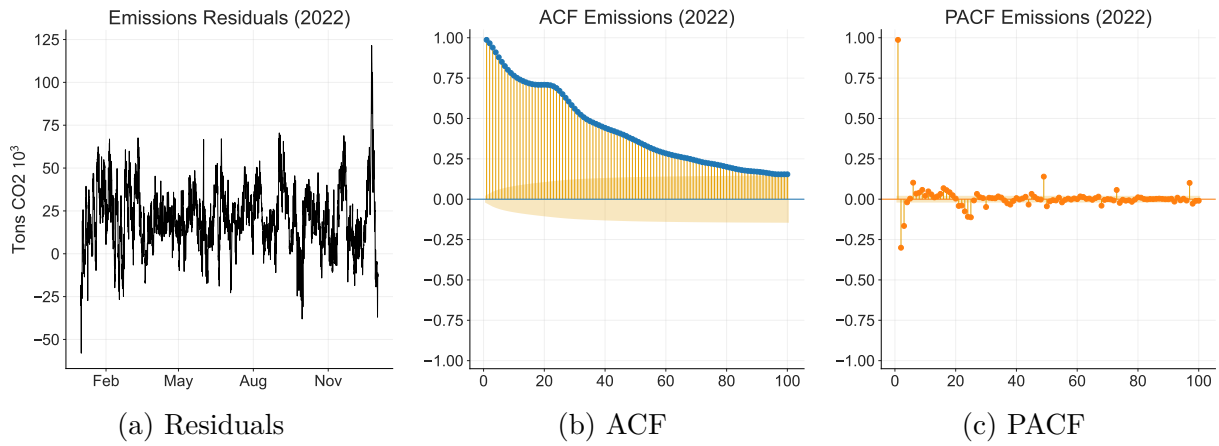


Figure S4: Diagnostic plots for **Emissions** (2022).

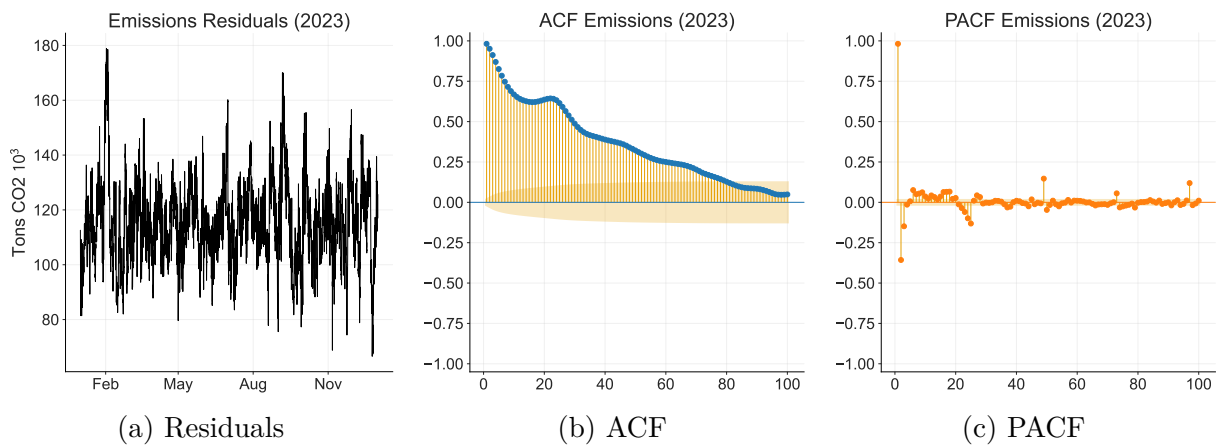


Figure S5: Diagnostic plots for **Emissions** (2023).

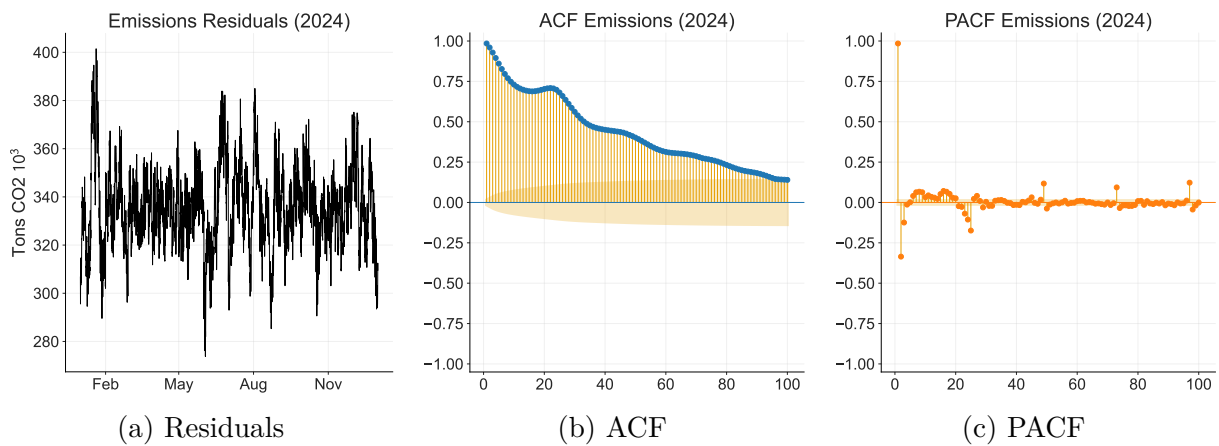


Figure S6: Diagnostic plots for **Emissions** (2024).

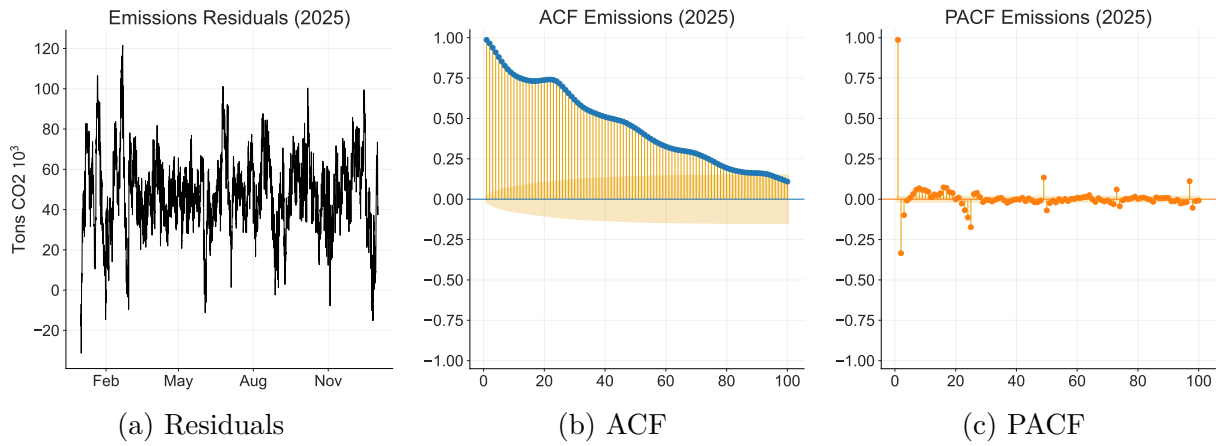


Figure S7: Diagnostic plots for **Emissions** (2025).

S4 Generation Diagnostics (2019–2025)

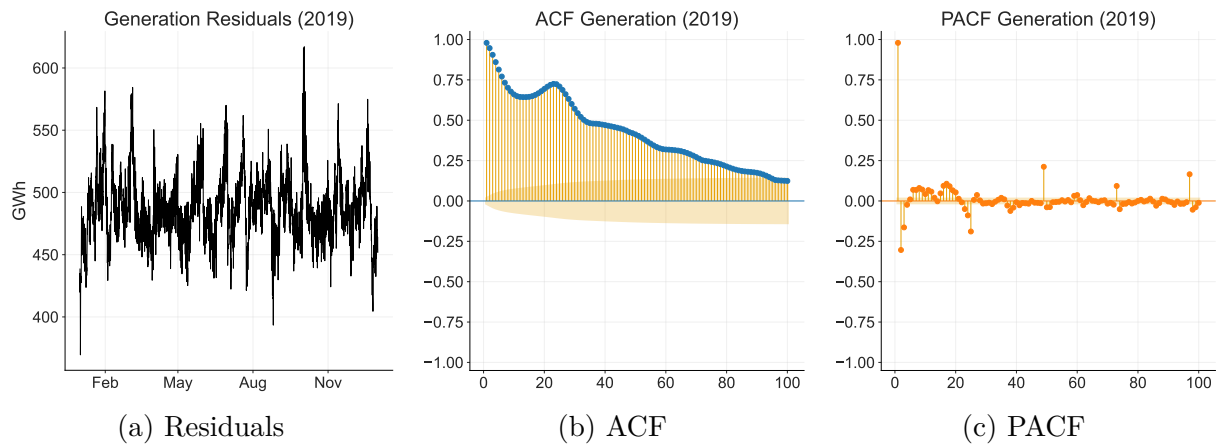


Figure S8: Diagnostic plots for **Generation** (2019).

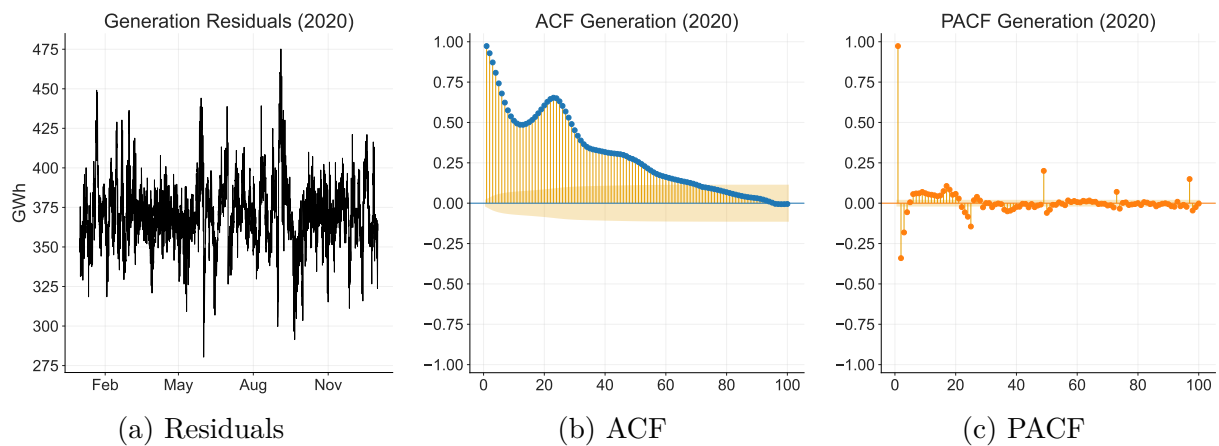


Figure S9: Diagnostic plots for **Generation** (2020).

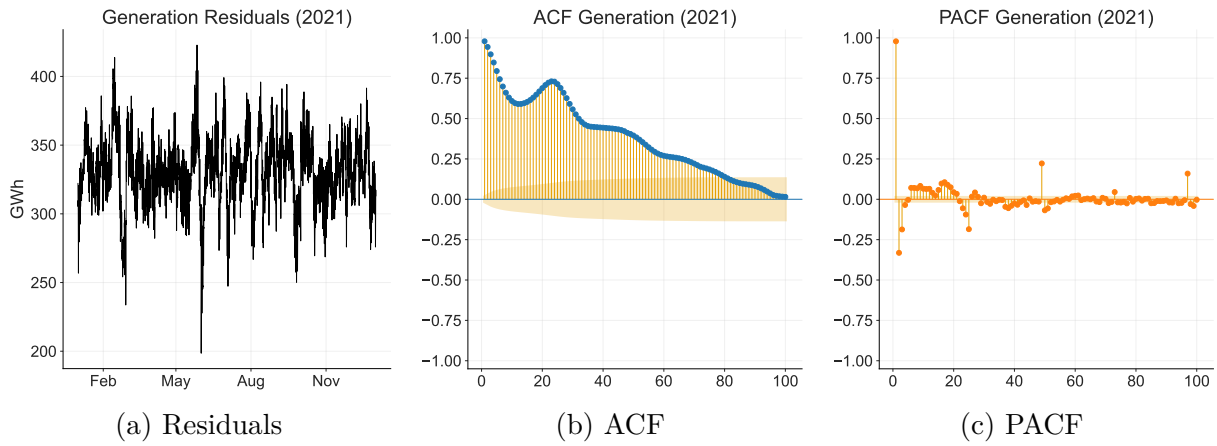


Figure S10: Diagnostic plots for **Generation** (2021).

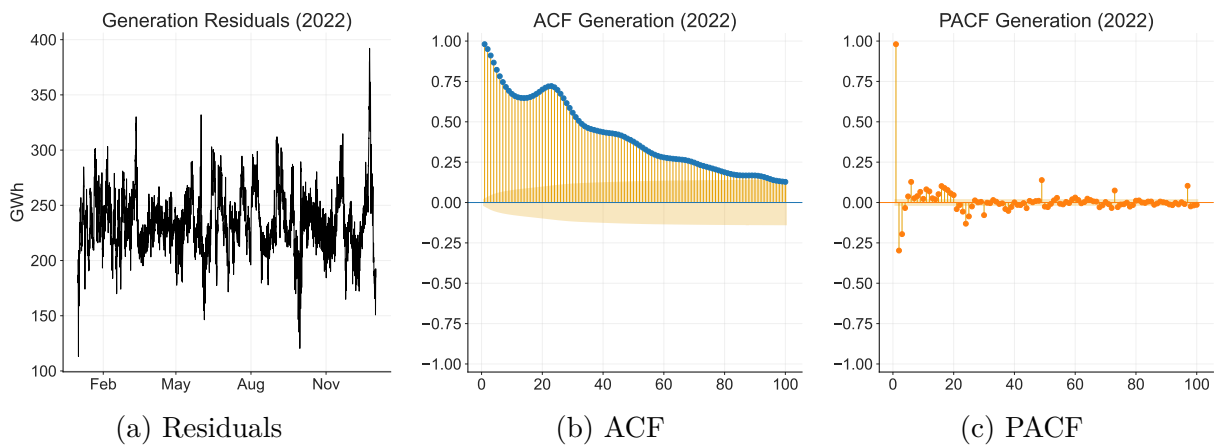


Figure S11: Diagnostic plots for **Generation** (2022).

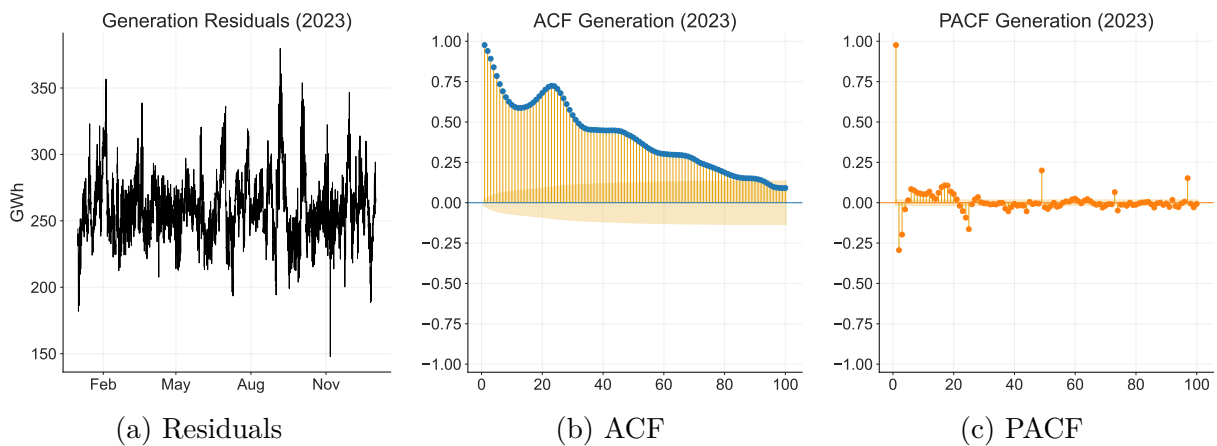


Figure S12: Diagnostic plots for **Generation** (2023).

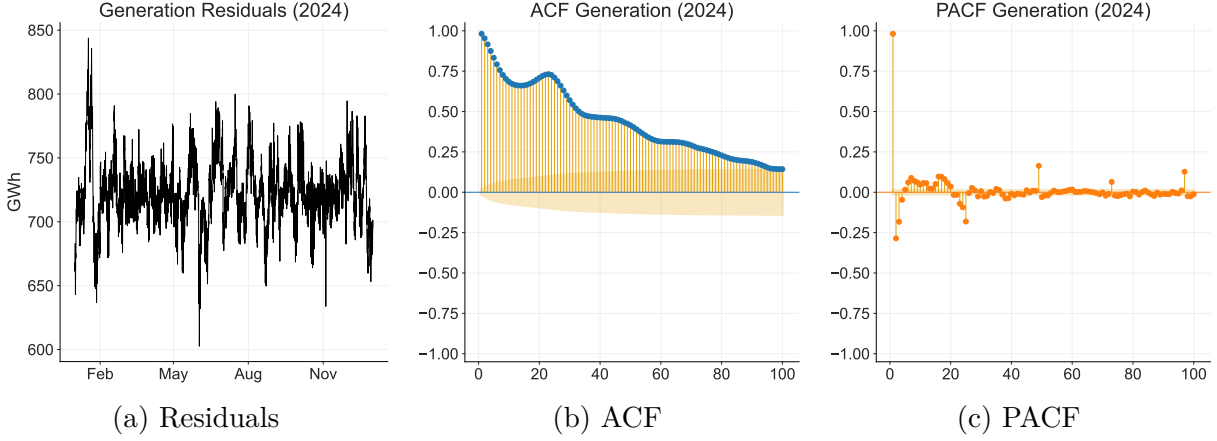


Figure S13: Diagnostic plots for **Generation** (2024).

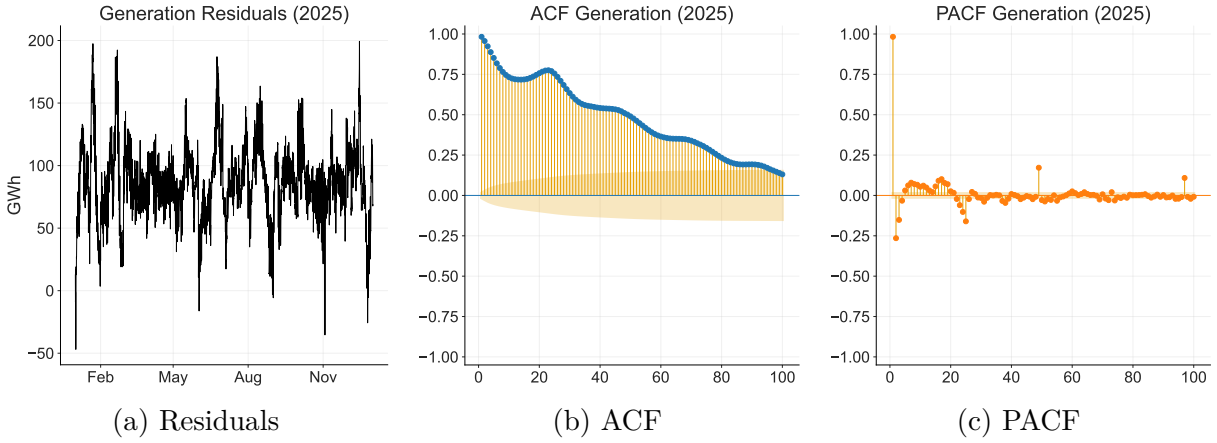


Figure S14: Diagnostic plots for **Generation** (2025).

S5 Autoregressive Order Selection

The selection of the autoregressive lag order (p) is a critical specification decision in regime-switching frameworks. While standard linear diagnostics (e.g., Partial Autocorrelation Functions) on the de-seasonalized series suggested potential higher-order dependence, these linear tools do not account for the non-linear dynamics introduced by regime switching. To rigorously determine the optimal lag structure, we systematically estimated MS-ARX specifications with $p \in \{1, 2, 3, 4\}$. The results of this sensitivity analysis are summarized in Table S4. We observe a clear trade-off between model complexity and numerical stability: Models with $p \geq 2$ systematically failed to satisfy convergence criteria. While these models report higher log-likelihoods and more favorable information criteria (AIC/BIC), these values are numerical artifacts of an unstable optimization. This convergence failure is a well-documented identification issue in regime-switching literature (Hamilton, 1990, and Krolzig, 1997) and arises from two sources: 1) higher-order lags exponentially increase the parameter space - an MS-ARX(2) model with $K = 2$ regimes requires estimation of $2K(p + 3)$ parameters - creating a highly non-convex likelihood surface prone to local optima; 2) autoregressive dynamics and regime persistence are observationally similar; the model cannot reliably distinguish whether emission persistence arises from AR(p) terms or from regime stickiness (high p_{11} , p_{22} transition probabilities).

Table S4: Convergence Diagnostics for MS-ARX Models with Alternative Lag Structures

p	Regimes	Log-Likelihood	AIC	BIC	HQIC
1	2	110,685.12	-221,348.25	-221,248.98	-221,317.45
2	2	113,571.17 [†]	-227,116.35	-226,999.03	-227,079.95
3	2	113,591.85 [†]	-227,153.69	-227,018.32	-227,111.69
4	2	113,644.60 [†]	-227,255.20	-227,101.79	-227,207.60

Note: All models were estimated with homoscedastic errors ($\sigma_1^2 = \sigma_2^2$).

[†] Likelihood values for non-convergent models. These values reflect local maxima or saddle points rather than global optima.

Consequently, the MS-ARX(1) specification is the highest-order model that achieves stable convergence. This selection is also theoretically consistent with power system dynamics: the AR(1) term captures the short-run physical inertia of the grid (e.g., thermal ramping constraints), while the Markov process absorbs the structural shifts in the merit order (e.g., the discrete switch between gas-margin and coal-margin states). We therefore proceed with the parsimonious MS-ARX(1) specification for the main analysis.

S6 Residuals Diagnostics (2019–2025)

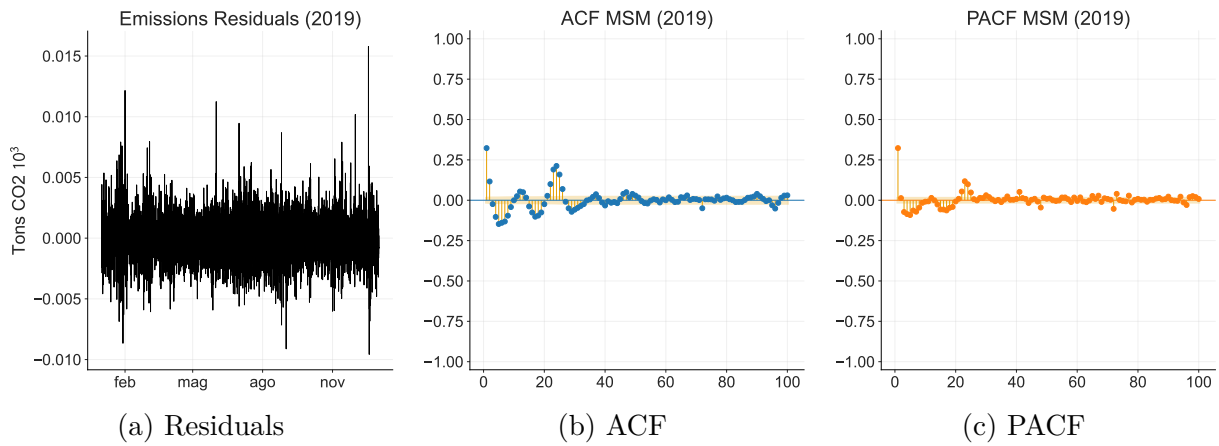


Figure S15: Diagnostic plots for MSM (2019).

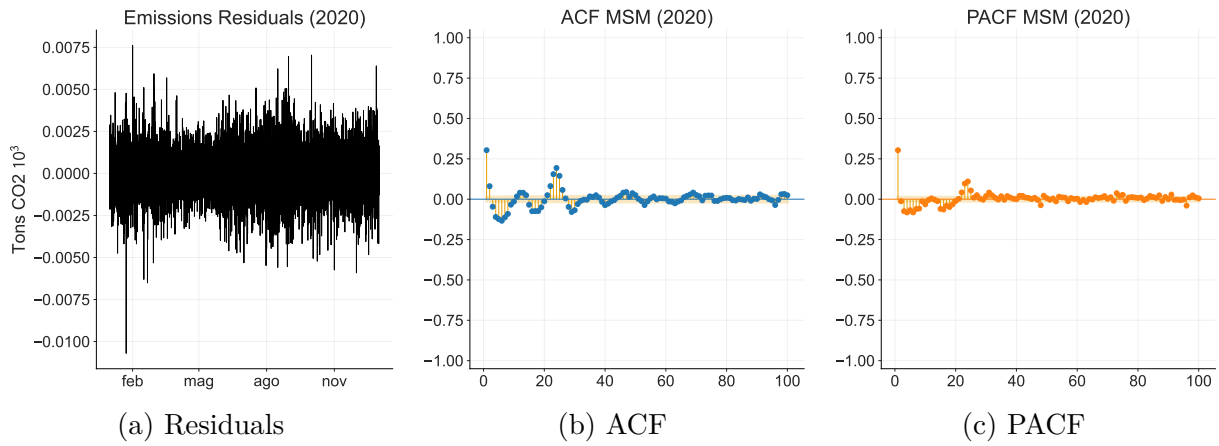


Figure S16: Diagnostic plots for MSM (2020).

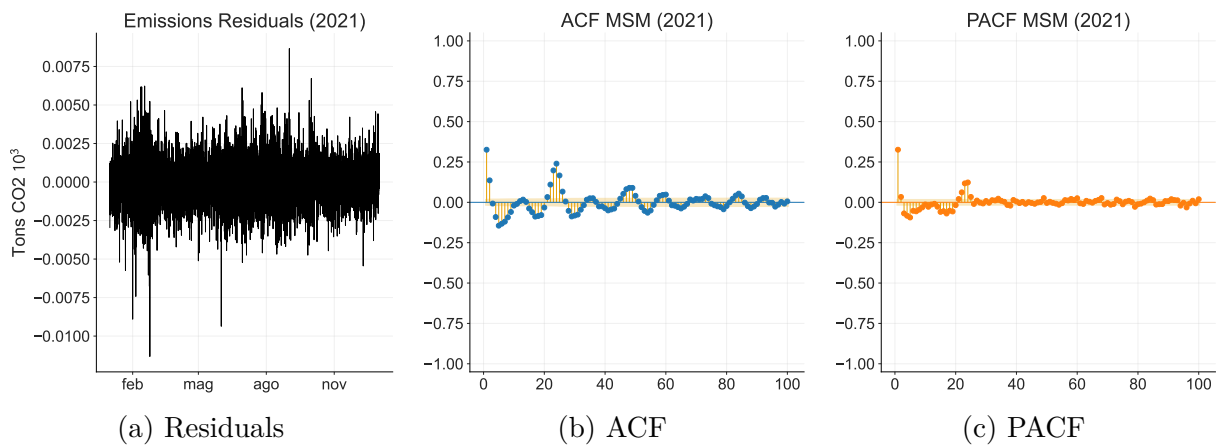


Figure S17: Diagnostic plots for MSM (2021).

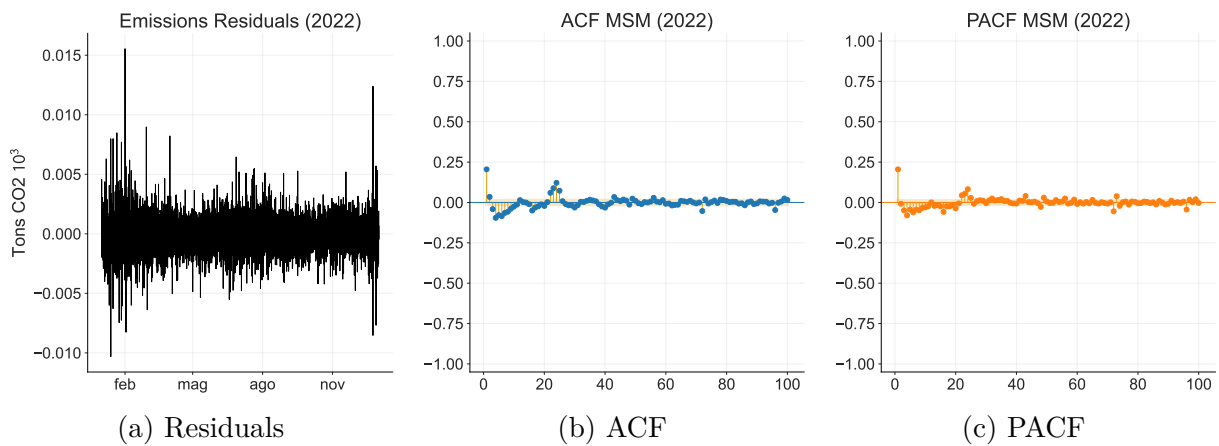


Figure S18: Diagnostic plots for MSM (2022).

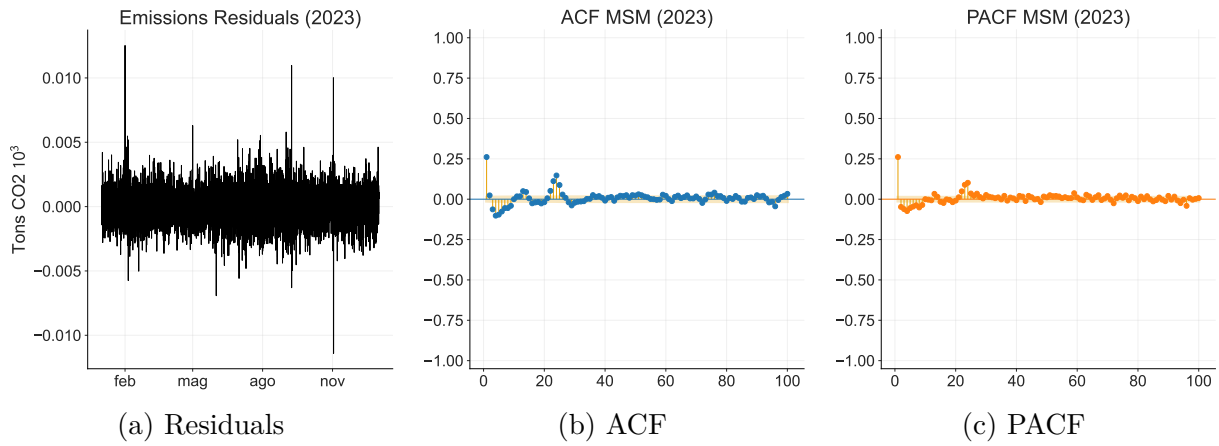


Figure S19: Diagnostic plots for MSM (2023).

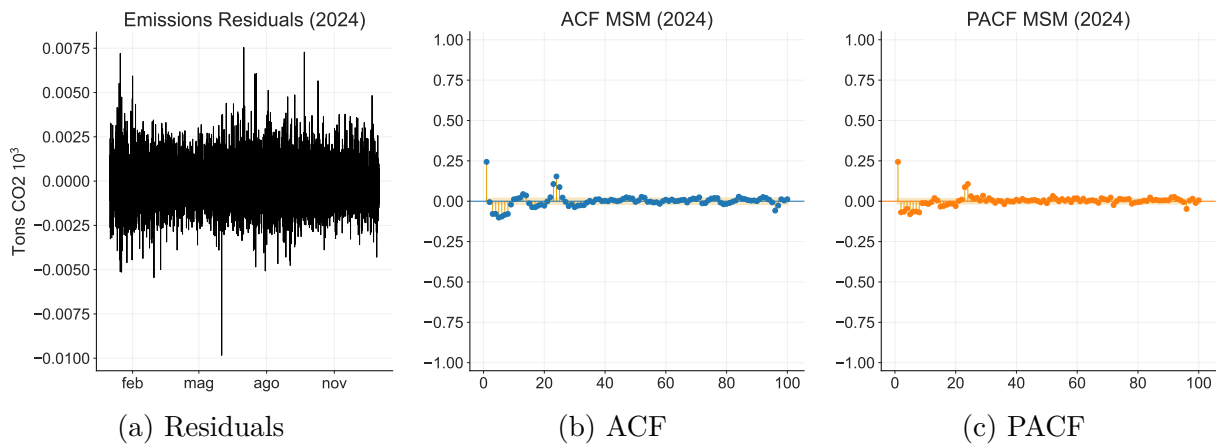


Figure S20: Diagnostic plots for MSM (2024).

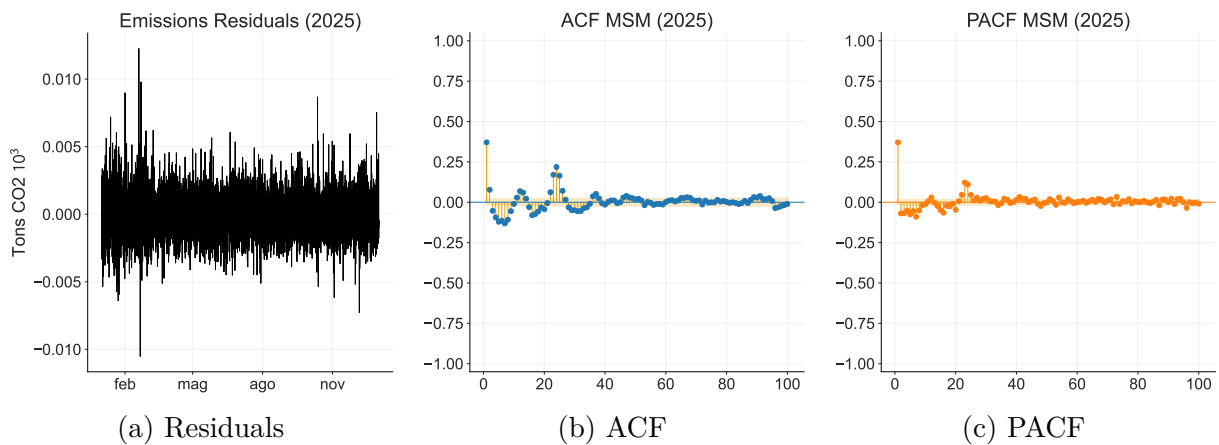


Figure S21: Diagnostic plots for MSM (2025).

S7 Comparative Analysis of Model Fit

To validate the selection of the Markov Switching Autoregressive model (MS-ARX), we compared its goodness-of-fit against two benchmark specifications: US-FE approach

(Holland and Mansur, 2008) and ARIMA model (Beltrami et al., 2020). To ensure the comparability of log-likelihood functions across different model classes, all specifications were fitted to the standardized series of hourly marginal emissions.

Table S5 summarizes the performance metrics. First, the results highlight that the static OLS framework lacks in explaining the data behavior, noting the wide gap between MSM-ARX(1) and ARIMA. The comparison between the dynamic specifications highlights a fundamental trade-off between statistical curve-fitting and economic structure.

The ARIMA(3,0,4) model achieves the highest statistical fit relying on a complex lag structure with seven temporal parameters. Although mathematically flexible, this specification imposes a restrictive assumption: it treats the data-generating process as a single, invariant linear mechanism, obscuring the physical reality of fuel switching.

The MS-ARX(1) model, employing a parsimonious first-order lag structure ($p = 1$), achieves a competitive fit with respect to ARIMA while explicitly modeling structural non-linearities. Although the ARIMA model offers a marginally superior statistical fit, its predictions average over distinct market conditions, leading the model to not have a useful economic specification.

Table S5: Goodness-of-Fit Comparison

Model Specification	Log-Likelihood	AIC	BIC	HQIC
ARIMA(3,0,4)	113,855.27	-227,688.55	-227,589.28	-227,657.75
MS-ARX(1)	110,685.12	-221,348.25	-221,248.98	-221,317.45
OLS (US-FE)	21,690.97	-43,375.94	-43,348.87	-43,367.54

Note: All models were fitted to the standardized series of hourly marginal emissions to ensure scale comparability of the log-likelihood functions.

S8 Annual Model Estimation Results

Table S6 details the estimated Marginal Emission Factors (MEFs) for each year from 2019 to 2025 across the different methodological approaches. The values represent the marginal CO₂ emissions (in lbs/MWh) induced by a unit increase in electricity demand. Standard errors are provided in parentheses.

We observe a consistent ordering among the benchmark models: the static Fixed Effects model (US-FE) consistently yields the highest MEF estimates (ranging from 1.37 to 1.50 lbs/MWh), while the dynamic approaches (Hawkes and ARIMA) provide more conservative estimates.

The Markov Switching results reveal significant heterogeneity hidden by the linear benchmarks. The *High-MEF* regime estimates remain robustly high (1.25 – 1.55 lbs/MWh) across all years, effectively capturing the "coal-on-margin" dynamics. In contrast, the *Low-MEF* regime shows substantial volatility. Notably, in 2019, the *Low-MEF* regime was 0.465 lbs/MWh, indicative of a gas-dominated margin. However, during the gas price inflationary period (2021-2022), the *Low-MEF* regime converged closer to the *High-MEF* regime (e.g., 1.28 lbs/MWh in 2021), reflecting the economic displacement of coal into the baseload and the increased marginality of less efficient units.

Table S6: Annual Marginal Emission Factors (lbs/MWh) by Model. Standard Errors are reported in parentheses.

Year	US-FE (OLS)	Hawkes (FD)	ARIMA	MS-High	MS-Low
2019	1.500 (0.016)	1.372 (0.002)	1.397 (0.002)	1.500 (0.004)	0.465 (0.113)
2020	1.415 (0.018)	1.327 (0.002)	1.368 (0.001)	1.412 (0.003)	0.916 (0.081)
2021	1.395 (0.017)	1.244 (0.002)	1.315 (0.001)	1.546 (0.014)	1.281 (0.003)
2022	1.390 (0.018)	1.219 (0.002)	1.275 (0.001)	1.255 (0.003)	0.891 (0.018)
2023	1.369 (0.017)	1.283 (0.001)	1.292 (0.001)	1.285 (0.003)	0.877 (0.044)
2024	1.415 (0.016)	1.292 (0.002)	1.311 (0.001)	1.341 (0.008)	1.297 (0.003)
2025	1.392 (0.012)	1.232 (0.002)	1.260 (0.001)	1.393 (0.004)	1.236 (0.009)

S9 Hourly Marginal Emission Factor (MEF) Results

The hourly Marginal Emission Factor (MEF) estimates for both operational periods are summarized in Table S7. The coefficients β_{low} and β_{high} represent the marginal impact of load on emissions, accompanied by their respective standard errors (SE) and the average system load (\bar{L}).

Table S7: Hourly MEF Summary: Pre-break and After-break Periods

Hour (h)	β_{low}	β_{high}	SE_{low}	SE_{high}	Avg. Load (\bar{L})
<i>Panel A: Pre-break Period</i>					
1	1.338	1.526	0.0085	0.0092	424 110
2	1.346	1.532	0.0087	0.0096	406 299
3	1.347	1.544	0.0085	0.0098	393 565
4	1.352	1.523	0.0086	0.0108	385 951
5	1.361	1.582	0.0070	0.0117	383 879
6	1.434	1.674	0.0062	0.0338	389 642
7	1.327	1.568	0.0051	0.0166	405 185
8	1.338	1.598	0.0051	0.0102	423 206
9	1.284	1.451	0.0063	0.0053	437 960
10	1.303	1.473	0.0059	0.0061	450 008
11	1.314	1.476	0.0059	0.0079	460 178
12	1.320	1.510	0.0056	0.0110	468 584
13	1.330	1.501	0.0061	0.0206	475 399
14	1.275	1.445	0.0072	0.0082	481 029
15	1.322	1.461	0.0062	0.0178	485 505
16	1.228	1.398	0.0097	0.0069	489 412
17	1.306	1.459	0.0063	0.0153	494 437
18	1.352	1.485	0.0075	0.0180	501 134
19	1.271	1.677	0.0051	0.0173	505 446
20	1.300	1.600	0.0051	0.0159	504 602
21	1.281	1.484	0.0072	0.0078	499 789
22	1.301	1.510	0.0072	0.0083	488 481
23	1.323	1.532	0.0071	0.0084	469 167
24	1.348	1.553	0.0075	0.0091	446 454
<i>Panel B: After-break Period</i>					
1	1.321	1.507	0.0056	0.0222	453 236
2	1.293	1.364	0.0085	0.0065	435 206
3	1.302	1.481	0.0064	0.0111	421 263
4	1.262	1.349	0.0173	0.0054	412 064
5	1.254	1.335	0.0259	0.0051	408 762
6	1.281	1.496	0.0054	0.0109	412 993
7	1.264	1.461	0.0055	0.0120	426 562
8	1.242	1.373	0.0070	0.0081	442 358
9	1.249	1.376	0.0074	0.0075	455 219
10	1.257	1.371	0.0082	0.0078	466 616
11	1.262	1.358	0.0086	0.0074	478 028
12	1.253	1.348	0.0099	0.0066	489 055
13	1.249	1.342	0.0111	0.0061	499 262
14	1.290	1.431	0.0046	0.0145	507 972
15	1.167	1.300	0.0348	0.0047	515 009
16	1.158	1.336	0.0641	0.0049	521 204
17	1.286	1.462	0.0051	0.0231	528 022
18	1.153	1.298	0.0241	0.0052	535 363
19	1.076	1.339	0.0653	0.0053	538 533
20	1.320	1.361	0.0181	0.0210	535 941
21	1.270	1.386	0.0079	0.0163	529 127
22	1.275	1.472	0.0050	0.0194	517 169
23	1.306	1.513	0.0052	0.0341	497 975
24	1.316	1.529	0.0060	0.0279	475 369

S10 Dummy MEF

Table S8 presents the estimated coefficients for the Markov-switching specifications defined in Equations (5) and (19). All parameters are statistically significant at the 1% level. Notably, the interaction terms (δ_{s_t}) are negative across both regimes, supporting our hypothesis that the structural break in natural gas prices following May 2022 has been beneficial in reducing marginal emissions.

Table S8: Comparison of MSM Model Coefficients

Variable	Model 1 (With Dummy)	Model 2 (Baseline)
Low MEF	1.2707 (0.0026)	1.2539 (0.0016)
High MEF	1.4544 (0.0036)	1.4361 (0.0039)
Dummy_Low	-0.1005 (0.0084)	–
Dummy_High	-0.0565 (0.0068)	–

Note: Standard errors are reported in parentheses.

Note: All coefficients are statistically significant at the 1% level.